

ADA021326

AFML-TR-75-217 ✓

12

6

CHEMISTRY OF HALIDE WINDOW GROWTH

Hughes Research Laboratories
3011 Malibu Canyon Road ✓
Malibu, CA 90265

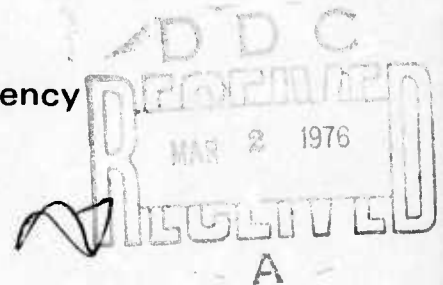
February 1976

Technical Report AFML-TR-75-217

Final Technical Report for period
1 April 1974 through 30 September 1975

APPROVED FOR PUBLIC RELEASE; DISTRIBUTION UNLIMITED

Sponsored by
Defense Advanced Research Projects Agency
1400 Wilson Boulevard
Arlington, VA 22209



Air Force Materials Laboratory
Air Force Wright Aeronautical Laboratories
Air Force Systems Command
Wright-Patterson AFB, OH 45433

DISCLAIMER NOTICE

THIS DOCUMENT IS THE BEST
QUALITY AVAILABLE.

COPY FURNISHED CONTAINED
A SIGNIFICANT NUMBER OF
PAGES WHICH DO NOT
REPRODUCE LEGIBLY.

DARPA Order Number	2612
Program Code Number	4D12
Contractor	Hughes Research Laboratories
Effective Date of Contract	1 April 1974
Contract Expiration Date	30 September 1975
Amount of Contract	\$243,936.00
Contract Number	F33615-74-C-5115
Principal Investigator and Telephone Number	R. C. Pastor (213) 456-6411
Title of Work	Chemistry of Halide Window Growth

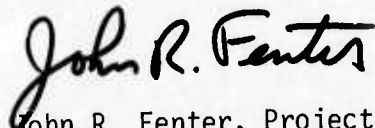
The views and conclusions contained in this document are those of the authors and should not be interpreted as necessarily representing the official policies, either expressed or implied, of the Advanced Research Projects Agency or the U.S. Government.

NOTICE

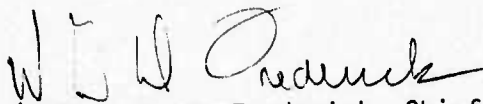
When Government drawings, specifications, or other data are used for any purpose other than in connection with a definitely related Government procurement operation, the United States Government thereby incurs no responsibility nor any obligation whatsoever; and the fact that the government may have formulated, furnished, or in any way supplied the said drawings, specifications, or other data, is not to be regarded by implication or otherwise as in any manner licensing the holder or any other person or corporation, or conveying any rights or permission to manufacture, use, or sell any patented invention that may in any way be related thereto.

This report has been reviewed by the Information Office (OI) and is releasable to the National Technical Information Service (NTIS). At NTIS, it will be available to the general public, including foreign nations.

This Technical Report has been reviewed and is approved.



John R. Fenter, Project Engineer
Laser and Optical Materials Branch
Electromagnetic Materials Division
Air Force Materials Laboratory



William G. D. Frederick, Chief
Laser and Optical Materials Branch
Electromagnetic Materials Division
Air Force Materials Laboratory

Copies of this report should not be returned unless return is required by security considerations, contractual obligations, or notice on a specific document.

UNCLASSIFIED

SECURITY CLASSIFICATION OF THIS PAGE (When Data Entered)

19 REPORT DOCUMENTATION PAGE		READ INSTRUCTIONS BEFORE COMPLETING FORM	
18 REPORT NUMBER AFML TR-75-217	2 GOVT ACCESSION NO.	3 RECIPIENT'S CATALOG NUMBER <i>Final technical rept. 1 Apr 74 - 30 Sep 75</i>	4
4 TITLE (and Subtitle) CHEMISTRY OF HALIDE WINDOW GROWTH.		5 TYPE OF REPORT & PERIOD COVERED Final Tech. Rpt. 1 Apr 1974 - 30 Sep 1975	
7 AUTHOR(s) R. C. / Pastor & H. V. / Winston		6 PERFORMING ORG. REPORT NUMBER	
9 PERFORMING ORGANIZATION NAME AND ADDRESS Hughes Research Laboratories 3011 Malibu Canyon Road Malibu, CA 90265		CONTRACT OR GRANT NUMBER(s) F33615-74-C-5115	
11 CONTROLLING OFFICE NAME AND ADDRESS Defense Advanced Research Projects Agency 1400 Wilson Boulevard Arlington, VA 22209		10 PROGRAM ELEMENT PROJECT, TASK AREA & WORK UNIT NUMBERS Program Code 4D12 ✓ ARPA Order-2612	
14 MONITORING AGENCY NAME & ADDRESS (if different from Controlling Office) United States Air Force Air Force Systems Command Wright-Patterson AFB, OH 45433		12 REPORT DATE Feb 1976	
16 DISTRIBUTION STATEMENT (of this Report) Approved for public release; distribution unlimited		15 SECURITY CLASS. (of this report) UNCLASSIFIED	
17 DISTRIBUTION STATEMENT (of the abstract entered in Block 20, if different from Report)		15a DECLASSIFICATION/DOWNGRADING SCHEDULE <i>(R) 77p.1</i>	
18 SUPPLEMENTARY NOTES			
19 KEY WORDS (Continue on reverse side if necessary and identify by block number) Laser Windows, Reactive Atmosphere Process, Nascent Halogen, Crystal Growth, Low Absorption, Bromides, Chlorides, and Fluorides.			
20 ABSTRACT (Continue on reverse side if necessary and identify by block number) We have studied the chemistry of reactive atmosphere processing (RAP) for the growth of crystals of chlorides, bromides, and halides*. The purity and freedom from extrinsic absorption obtained by RAP are important in the application of halides as optical elements in high power lasers. → <i>* was studied</i>			

DD FORM 1 JAN 73 1473

EDITION OF 1 NOV 65 IS OBSOLETE

UNCLASSIFIED
SECURITY CLASSIFICATION OF THIS PAGE (When Data Entered)

172 600

mt

The prototype of RAP is CCl_4 in the growth of KCl; it reacts directly with water to scavenge out all traces of this contaminant and pyrolyzes with the formation of nascent halogen to react rapidly with hydroxide ions in the melt. ~~Our~~ approach with the bromides and fluorides has been to seek RAP agents which simulate the behavior of CCl_4 with KCl.

On the basis of its hydrolysis behavior, we selected $\text{CH}_2\text{Br}_2/\text{He}$ as the RAP agent for KBr. This has consistently yielded material with a $10.6 \mu\text{m}$ bulk absorption coefficient of $2 \times 10^{-4} \text{ cm}^{-1}$, an order of magnitude below that of non-RAP KBr. Further improvement is possible, there are indications of incomplete hydroxide ion removal such as partial sticking of the crystal ingot to the silica crucible and fogging of crystal surfaces on exposure to the environment. One calorimetry run gave a bulk absorption coefficient as low as $2 \times 10^{-5} \text{ cm}^{-1}$. In addition, we have found that the minimum-melting solid solution of NaBr and KBr prepared under RAP conditions does not retain phase homogeneity below the melting point, making it impossible to grow single crystals of this material.

We directed our work on KCl toward problems associated with the scale up of RAP to produce KCl crystals of greater than 10-cm diameter. The longer processing time required for larger crystals results in an accumulation of C and Cl_2 from the pyrolysis of CCl_4 . Deposited carbon can be included in the final crystal, and the buildup of Cl_2 leads to corrosion of the growth apparatus. We have employed admixtures of CO_2 and variations in the concentration of CCl_4 in attempts to control these problems. The results provide a basis for further actual large-scale crystal growth experiments.

Hydrogen fluoride, previously used alone as a RAP agent for fluoride crystal growth, is fast acting but does not achieve a low RAP index, $\text{P}(\text{H}_2\text{O})/\text{P}(\text{HF})$. We have supplemented it with a fluorocarbon, and an achieved improved transparency with CF_4 admixtures. Carbon tetrafluoride is the actual agent present when C_2F_4 from the decomposition of Teflon is used in RAP, since C_2F_4 breaks down into CF_4 at temperatures below the melting points of the alkaline earth fluorides. Thus, teflon may be regarded as an inexpensive source of CF_4 for RAP.

* $1/\phi\phi\phi 2 \text{ cm}$

** It was found
*** Supplementing

TABLE OF CONTENTS

SECTION		PAGE
I	INTRODUCTION	1
II	BACKGROUND	3
III	RAP CHEMISTRY AND CRYSTAL GROWTH	7
	Task A: Bromides	7
	Task B: Chlorides (KCl)	12
	Task C: Fluorides (MF ₂ and Solid Solutions)	13
IV	EVALUATION	23
	Task A: Bromide (KBr)	23
	Task B: Chloride (KCl)	23
	Task C: Fluoride (MF ₂ and Solid Solutions)	29
V	CONCLUSIONS AND RECOMMENDATIONS	37
	APPENDIX A - Crystal Growth in a Reactive Atmosphere	39
	APPENDIX B - Crystal Growth of KBr in a Reactive Atmosphere	47
	APPENDIX C - Crystal Growth of KCl in a Reactive Atmosphere	53
	APPENDIX D - Crystal Growth of Alkaline Earth Fluorides in a Reactive Atmosphere	59
	APPENDIX E - Approach to Equilibrium in the Dissociation of X ₂	67
	REFERENCES	71

LIST OF ILLUSTRATIONS

FIGURE		PAGE
1	Pyrolysis of CBr_4/He and CCl_4/He at 800°C	8
2	Single-crystal ingots of the minimum- melting solid solutions of the alkaline earth fluorides	17
3	Temperature dependence of the decay constant (k) for the depolymerization of TFE under various atmospheres	20
4	Infrared transmission of KBr single crystals	24
5	Infrared transmission of a 12.2 cm long KCl single-crystal ingot grown in CCl_4/CO_2	27
6	Infrared spectrum of single crystal BaF_2 grown in HF/He	30
7	Infrared spectrum of single crystal SrF_2	33
8	Infrared spectra of single-crystal, minimum-melting, solid solutions of the alkaline-earth fluorides	34
A-1	Schematic of pyrolysis apparatus	42
A-2	Sublimation of CBr_4 versus temperature	44
A-3	A 10-cm diameter single-crystal KCl grown by RAP-Bridgman with CCl_4 in He at a flow of $\sim 0.5 \text{ cm}^3/\text{s}$	45
B-1	RAP grown single crystal KBr	51
C-1	Bridgman KCl ingots grown under CCl_4/He and CCl_4/CO_2	56
D-1	Crystal growth of MF_2	61
D-2	Transmission of RAP Crystals	62

I. INTRODUCTION

This program is a study of reactive atmosphere processing (RAP) chemistry, applied to metal halide crystal growth. The ultimate application of the crystals is as optical windows and components for 10 μm (chlorides and bromides) and 2 to 6 μm (fluorides). The object of the study is to establish the thermal decomposition (pyrolysis) behavior of candidate RAP agents and then to choose the RAP agent with the thermal behavior best suited to the processing and crystal growth requirements of a given metal halide. The study is divided into three tasks: Task A, bromides; Task B, chlorides; and Task C, fluorides.

Our general approach is to find compounds of the appropriate halogen which behave as CCl_4 does with KCl; good RAP agents should react directly with water to scavenge all traces of this universal contaminant as well as pyrolyze with the formation of nascent halogen to react rapidly with hydroxide ions in the melt. Additional requirements are freedom from crucible corrosion and the possibility of complete removal of pyrolysis products that might interfere with crystal growth.

The objective in Task A is to develop a RAP growth procedure for KBr and its congruent-melting solution with NaBr. These materials are of interest for window use in the 10 μm region. The RAP growth recipes are based on the results of pyrolysis studies of CBr_4 and its derivatives.

The objective in Task B is to optimize the RAP chemistry and growth procedure for the scaled-up growth of larger crystals of KCl (≥ 10 cm diameter), another 10 μm window material. Although CCl_4 works as a RAP agent the larger processing time necessary in scaled-up growth leads to various problems arising from the accumulation of C and Cl_2 from the pyrolysis of CCl_4 . The deposited carbon may be a contributing factor to significant deviations of the ingot from monocrystallinity and, not infrequently, reduces the utilizable fraction. The smaller carbon particles remain suspended in the melt and become inclusions in the crystal which lower the 10.6 μm laser-damage threshold of the crystal. Excessive buildup of Cl_2 limits the lifetime of the growth apparatus.

The objective in Task C is to improve the RAP recipe for the growth of alkaline earth fluorides and its solid solutions, i. e., mixed cation fluorides. These materials are of interest for window use in the 2 to 6 μm region. In the past, RAP growth was carried out with HF, which we now realize is an inadequate RAP agent. Because of outgas, the RAP-index, $P(\text{H}_2\text{O})/P(\text{HF})$, during growth is three orders of magnitude larger than the H_2O -content of the HF gas in the cylinder (see Appendix D). Consequently an additional vapor-phase reactant is needed to react with H_2O , preferably, to convert H_2O to HF.

II. BACKGROUND

The elimination of impurities is an obvious prerequisite for the preparation of highly transparent materials. Anion purity is a prime concern for high-power infrared window materials, because anions, particularly polyatomic ones, contribute significantly to infrared absorption through the fundamentals and combinations of their vibrational modes.¹ However, many of these anions pyrolyze at temperatures below the melting point of the halide. Those anions which are thermally stable are readily decomposed or displaced by treatment of the melt with the hydrogen halide (HX) gas. Prolonged treatment is not required when the sources of impurities are extremely limited.

The hydroxyl ion, OH^- , and related impurities (oxides and oxyhalides) are the most troublesome because of the ubiquitous nature of their source (H_2O),



Consequently, the central theme of reactive atmosphere processing (RAP) is control of the RAP-index, $\text{P}(\text{H}_2\text{O})/\text{P}(\text{HX})$, the key parameter for reducing the hydroxide/halide ratio in the crystal:

$$\frac{[\text{OH}^-]}{[\text{X}^-]} = K \frac{\text{P}(\text{H}_2\text{O})}{\text{P}(\text{HX})} \quad (2)$$

The proportionality constant, K , is a steady-state parameter whose value depends on the reaction paths available in RAP. When these path rates are great enough for the steady-state balance to approximate the equilibrium condition, then K becomes the equilibrium constant of the mass-action relation of eq. (1).

In Appendix A, we consider RAP paths based on the use of HX , X_2 , COX_2 , and CX_4 . All these agents, except HX , provide for the formation of two moles of HX at the expense of one mole of H_2O . Hence HX by itself is apt to be an inadequate RAP agent because the RAP index is severely limited by the uncontrolled sources of H_2O .

Aside from the RAP-index consideration, which shows that all HX are inadequate RAP agents, HF is the poorest agent in the HX group for RAP growth by eq. (1). In contrast to HCl, HBr, and HI, the free energy of formation (ΔG) of HF is lower than that of H_2O . With increasing T, $\Delta G(HF)$ decreases while $\Delta G(H_2O)$ increases. In the alkaline-earth halides, the fluorides have the lowest ΔG and the highest melting point. For example, the equilibrium constants for eq. (1) of the calcium halides at their respective melting points are CaF_2 , $K = 0.055$; $CaCl_2$, $K = 0.0034$; $CaBr_2$, $K = 0.0052$; and CaI_2 , $K = 0.018$. A higher value of K in eq. (1) means a higher degree of hydrolysis. The calculation of K is given in detail in Interim Report 1.²

The basis for selecting the reactions of X_2 , COX_2 , and CX_4 was the thermodynamic value of the RAP index. This calculation of the RAP index deals only with homogeneous RAP, i. e., the gas phase, and appears to be a good first approximation at the higher operating temperatures where reaction rates are large. At the growth temperature, the rates tending to equilibrate the condensed phases (melt and crystal) with the vapor are much faster than the growth rate. This coupling of rates in the heterogeneous system enables the gas phase to act as the impurity sink, hence the utility of the RAP index.

Appendix A provides a comparison of the RAP-index for chlorides, i. e., Cl_2 , $COCl_2$, and CCl_4 , from 600 to 1200°K. Both $COCl_2$ and CCl_4 are far superior to Cl_2 as RAP agents. Carbon tetrachloride is preferred to $COCl_2$ because it is less toxic and easier to handle.

Another advantage to the use of CX_4 as the RAP agent is the pyrolytic generation of the nascent halogen (X). All the nascent halogens, i. e., $X = F, Cl, Br, \text{ and } I$, have a higher electron affinity than the OH radical and, therefore, will be potent agents for the displacement of OH^- in the melt (see Appendix A).

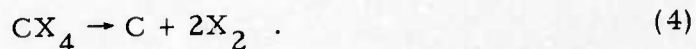
However, pyrolysis temperature depends upon the vibration frequency and dissociation energy of the C-X bond. If pyrolysis occurs at a temperature far below the melting point of the halide, the recipe is impractical. The nascent halogen is rapidly converted to the

molecular (diatomic) form which, except for F_2 , is ineffective for RAP growth. At the halide melting point, although the equilibrium approach to dissociation $X_2 \rightleftharpoons 2 X$, is fast, the extent of dissociation is small (see Appendix E). Thus, at $1000^\circ K$ the time required to reach the half-point of equilibrium and the degree of dissociation are as follows: F_2 , 3.5×10^{-7} sec and 4.3%; Cl_2 , 7.1×10^{-5} sec, 0.035%; Br_2 , 2.2×10^{-6} sec, 0.23%; and I_2 , 2.7×10^{-7} sec, 2.8%.

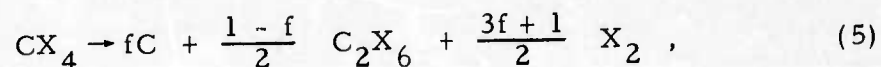
From the preceding discussion, it is clear that the CX_4 pyrolysis path useful to RAP is



The undesired path is



These two paths compete and the dominance of one over the other depends on temperature. This competition is summarized in the following total reaction



where $f = 0$ is eq. (3) and $f = 1$ is eq. (4). The object in RAP chemistry is to attain an f value close to zero at the melting point of the metal halide in question.

The schematic of the pyrolysis apparatus and the procedure followed to determine f versus temperature is given in Appendix A.

III. RAP CHEMISTRY AND CRYSTAL GROWTH

Task A: Bromides

Pyrolysis studies with He as the carrier gas showed that the f value of CBr_4/He was very close to unity at 700°C (see Appendix B). Hence, at the melting point of KBr ($\text{mp} = 730^\circ\text{C}$), the halogen would be in the molecular form (Br_2) accompanied by a heavy deposit of carbon. This striking difference in pyrolysis behavior between CBr_4/He and CCl_4/He is shown in Fig. 1.

To provide a quick test for the suitability of RAP agents, the pyrolysis chamber was replaced with a horizontal silica tube. Silica boats loaded with KBr powder were melted under a flow of $1 \text{ cm}^3/\text{sec}$ of RAP agent/He. At the given flow, the pyrolysis residence time was 200 sec. With this test apparatus, it was established that neither CBr_4/He nor CHBr_3/He was suitable for RAP growth of KBr.

The C-Br bond dissociation energy (D) increases with the extent of replacement of bromine by a more strongly covalent-bonded substituent: CBr_4 , 49; CHBr_3 , 56; CH_2Br_2 , 63; CF_3Br , 65; and CH_3Br , 67 (unit of D in kcal).³ The C-Br dissociation has been shown to be characterized by

$$k = \nu \exp(-D/RT) \quad , \quad (6)$$

where ν and D are the C-Br vibration frequency and dissociation energy, respectively.⁴ The value of $\nu = 1.75 \times 10^{13} \text{ s}^{-1}$ (Ref. 5).

At the RAP growth temperature, pyrolysis should be constrained to $0 < k < 1$. At $k = 1$, the agent would pyrolyze completely in the vapor phase; the halogen reaching the melt would be in the molecular form. From eq. (6) at 730°C (KBr mp), $k < 1$ if $D > 61$ kcal and this would explain why CBr_4 and CHBr_3 were inadequate.

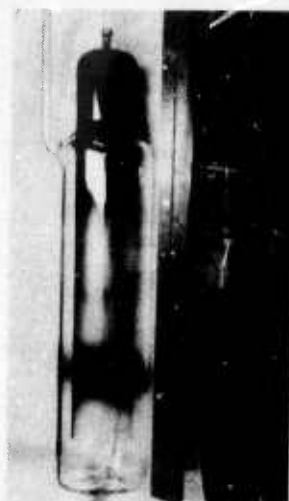
The two RAP agents which gave encouraging results in experiments on the melting of KBr were CH_2Br_2 and CF_3Br . Pyrolysis measurements showed that CH_2Br_2 was a poorer source of nascent bromine than CF_3Br (see Appendix B). Observation of the nonwetting

CARRIER GAS: He

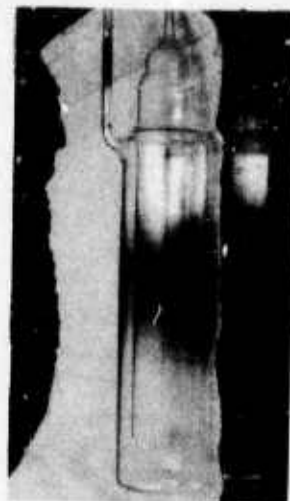
SOURCE TEMPERATURE : 24°C



PYROLYSIS
APPARATUS



PYROLYSIS OF CBr_4
AT 800°C/20 h
INPUT = 2.55×10^{-8}
MOLE CBr_4/cm^3



PYROLYSIS OF CCl_4
AT 800°C/20 h
INPUT = 5.40×10^{-6}
MOLE CCl_4/cm^3

Figure 1. Pyrolysis of CBr_4/He and CCl_4/He at 800°C.

behavior of KBr melt with the silica crucible showed CF_3Br to be more effective than CH_2Br_2 in scrubbing the melt.

However, the melting experiments only exposed the material to RAP for time intervals two orders of magnitude smaller than in crystal growth. We encountered severe corrosion of the crucible (silica) with $\text{CF}_3\text{Br}/\text{He}$ when we attempted the growth of 1.6 cm diameter KBr. Infrared transmission measurement on the crystal indicated contamination, possibly, with fluoride.

With increasing temperature, CH_2Br_2 pyrolysis favors the formation of HBr and decreases the bromine output (see Appendix B). Bromine is detected at the exit at 200°C . Its concentration increases with temperature up to 500°C and then drops with further increase in temperature. At 500°C , $\text{HBr}:\text{Br}$ is ~ 10 , at 700°C the ratio is $\sim 10^2$ and at 900°C , $\sim 10^3$. In spite of the large difference in concentration, the Br output from C-Br dissociation may actually be increasing with temperature but is readily converted to HBr by collision with CH_2Br_2 . On the other hand, the result may signify the activation of another breakdown path, the direct molecular split of HBr from CH_2Br_2 .

The latter alternative is favored by the results of pyrolysis of $\text{CH}_3\text{Br}/\text{He}$. No free halogen was detected in the gas effluent from 400 to 1000°C . The effluent HBr concentration showed the amount of CH_3Br pyrolyzed: $< 0.1\%$ at 400°C , $51 \pm 3\%$ at 600 to 800°C , and 60% at 1000°C . Since this dominant path does not involve nascent bromine, CH_3Br is not a good RAP agent for the growth of KBr.

In view of the above results, Bridgman crystal growth of KBr (1.6 to 4 cm diameter ingots) was carried out in $\text{CH}_2\text{Br}_2/\text{He}$. Higher melt-soak temperatures (800 to 900°C) were employed. This measure reduced but did not eliminate crucible (silica) wetting. This limitation on the reactivity of the RAP mixture, imposed by silica crucible corrosion, was avoided by the use of carbon (graphite) crucibles. With the latter the ingots grown were 5.3 cm in diameter.

Various NaBr-KBr mixtures, in a concentration range straddling the minimum-melting composition,⁶ were melted in conical crucibles under $\text{CF}_3\text{Br}/\text{He}$. After a few hours soak, followed by a slow cool under RAP, the specimens were examined with the DuPont 900 Thermal Analyzer and characterized by Knoop hardness measurement and x-ray powder diffraction.

Table 1 shows the results of the DTA and hardness measurements. DTA measurement of the freezing and melting of the mixtures showed a solid solution with a minimum. The observed minimum melting temperature under RAP is 620°C at 48 mol% KBr while the literature gives 644°C and 53 mol% KBr.⁶ In spite of this difference, our melting point determinations for NaBr and KBr showed no difference between the untreated and the RAP-treated material. Our mean value for the melting point of NaBr disagrees with certain literature values (see footnote (b) of Table 1) and Wicks and Block,⁷ who assign a melting point of 747°C , but agrees with the more recent assignment by Stull and Prophet.⁸

If the solid-solution phase persisted through cooldown, the Knoop hardness value would exhibit a broad maximum at the minimum melting composition. The third column of Table 1 shows that this is not the case. The hardness values shown were limited by the texture of the material, which was very turbid, suggesting the separation (precipitation) of other solid phases.

To test the latter hypothesis, we examined small ingots of the frozen mixture by x rays. The ingots were ground to provide a 1 cm^2 flat area for use in the x-ray analysis. Diffraction patterns were made on the Norelco diffractometer with filtered $\text{CuK}\alpha$ radiation. The patterns obtained from the ingots had intensity ratios for NaBr and KBr which were proportional to the ratios derived from the starting compositions, i. e., the material behaved like a mechanical mixture of NaBr and KBr. The position of the lines did not shift, which also indicates that there was very little solid solubility of one component in the other.

TABLE 1. MELTING POINT AND KNOOP HARDNESS OF NaBr-KBr MIXTURES

Mole % KBr	Melting Point, °C	Knoop Hardness, ^(a) kg/mm ²
0	737 ± 2 ^(b)	7 to 8 ^(c)
25	— ^(d)	3.4 to 5.8
40	629	0.2 to 0.3
45	621	0.3 to 0.4
50	621	0.4 to 0.6
55	629	0.5 to 0.7
60	635	1.5 to 3.2
75	— ^(d)	— ^(e)
100	732 ± 2 ^(b)	9.9 to 10.7 ^(f)

(a) Measured with a 15 g load unless specified otherwise.

(b) The range covers that obtained by direct melting of the reagent-grade powder and that obtained from the same material by RAP growth: NaBr in CHBr₃/He and KBr in CH₂Br₂/He. The literature values are 755°C for NaBr and 730°C for KBr; taken from Handbook of Chemistry and Physics, edited by R. C. Weast, 49th Edition (The Chemical Rubber Co., 1968-1969).

(c) Measurement made with 15, 25, and 50 g loads.

(d) Melting point not determined.

(e) Surface texture too crumbly to warrant a hardness measurement.

(f) A Knoop hardness of 7.0 kg/mm² is reported for the RAP-untreated KBr on page 13 of Harshaw Optical Crystals, (The Harshaw Chemical Company, 1967).

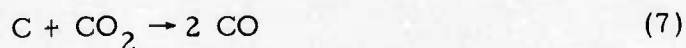
Our results on the minimum-melting solid solution of NaBr-KBr under RAP differ from the literature because (1) the temperature and concentration are lower, and (2) phase homogeneity does not persist below the melting point. The second difference is crucial to the objective of attaining single-crystal growth; it is clearly not possible to grow single crystals of the minimum-melting solid solution.

Task B: Chlorides (KCl)

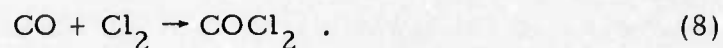
The pyrolysis of CCl_4/He shows $f = 0.21 \pm 0.01$ from 700 to 900°C (see Appendix A). Although only one of every five molecules of CCl_4 decomposes by eq. (4), the undesired path, considerable carbon and molecular halogen (Cl_2) accumulate even in the growth of 0.4 kg KCl (3.2 cm diameter crystal). A lower rate of formation of these undesired products is needed in crystal growth on the 4-kg scale (10 cm diameter crystal).

Two approaches are possible to reduce the formation of C and Cl_2 . The f value may be lowered further by decreasing the mole ratio of $\text{CCl}_4:\text{He}$. This measure will reduce the CCl_4 -to- CCl_4 collisions but will not affect the specific decomposition rate of eq. (3), a first-order reaction.⁴ However, we do not know the effect of dilution on eq. (4). A gain is expected if the rate of eq. (4) depends on the collision frequency of CCl_4 to CCl_4 or CCl_4 to wall.

The other alternative is to accept the f value and employ a carrier component reactive to C and Cl_2 . We investigated this alternative and compared the pyrolysis behavior of CCl_4/He and CCl_4/CO_2 (see Appendix C). At 500°C , the rate of halogen formation is 200% higher in CO_2 . This feature may be explained by the difference in molecular mass and heat capacity of the carriers, CO_2 being the more efficient thermalizing agent. The difference in the rate decreases with increase in pyrolysis temperature; the crossover is at 700°C . Above 700°C , the rate of halogen formation increases when the carrier is He but decreases with CO_2 . This behavior is due to the reaction



and the resulting CO tying up free chlorine,



The decrease in free halogen content of the exit gas is explained by eq. (8), which is dependent on eq. (7). To assess the efficiency of eq. (7), a 20-hour pyrolysis at 800°C was carried out. No a carbon deposit formed in the case of CCl_4/CO_2 . This feature was reproduced in crystal growth (see Appendix C, Fig. 1).

Window specimens, 10 cm in length, were fabricated from these crystals. For both specimens, the infrared transmission (Beckman IR 12) was flat at 94% transmission from 2.5 to 12.5 μm with the knee of the curve at 14.5 μm . In the 10 μm region the differences are $\leq 0.5\%$ which indicates that the absorption coefficient at 10.6 μm would differ by $\leq 0.0005 \text{ cm}^{-1}$ between the two specimens. This difference could be accounted for by surface fabrication.

The results of infrared transmission measurements are significant to the objective of RAP growth, viz., removal of anion impurities. With CO_2 as the carrier, the presence of O^- and OH^- impurities in the melt would have led to the formation of CO_3^- and HCO_3^- impurities, respectively: $\text{CO}_2 + \text{O}^- \rightarrow \text{CO}_3^-$ and $\text{CO}_2 + \text{OH}^- \rightarrow \text{HCO}_3^-$.

In 10 cm length KCl, 100 ppm CO_3^- would have shown absorption bands from 6.6 to 14.7 μm , while 0.1 ppm HCO_3^- would have given absorption bands from 3.0 to 15.9 μm .¹ It can be shown that the $\text{HCO}_3^-/\text{CO}_3^-$ ratio depends on OH^-/O^- which, in turn, depends on H_2O . Hence, the results obtained indicate that the RAP procedure provided a very low value of the RAP index.

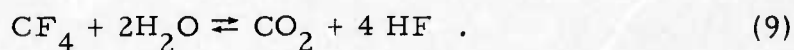
Task C: Fluorides (MF_2) and Solid Solutions

In Section II we discussed the thermodynamic basis for HF being the poorest HX RAP agent. However, among all the RAP agents, HX reacts with O^- and OH^- with the lowest energy barrier. It is the only agent capable of efficient halide conversion at room temperature. The product of the reaction, H_2O , must be removed to achieve a higher

degree of conversion. Because of the uncontrolled sources of H_2O in RAP growth, e. g. , outgas (see Section I), it is clear that a secondary RAP agent is needed to lower the RAP index.

Many hydrolyzable fluoride gases can convert one mole of H_2O to two moles of HF, e. g. , BF_3 , PF_5 , SF_6 , and CF_4 . We considered CF_4 and other fluorocarbons because these agents are less likely to cause complicating side reactions in our carbon resistance growth furnace.

We studied the reaction of CF_4 with H_2O , using both 5 mol% CF_4 in He and pure CF_4 , at a flow rate of $0.4 \text{ cm}^3/\text{sec}$, in a graphite reaction chamber,



The HF content of the effluent was chronometrically titrated by bubbling through a standard $NaHCO_3$ solution, using bromcresol green as the indicator.

Table 2 is a summary of the results. The first-row data are for outgassed H_2O only. At $900^\circ C$ and at an effluent flow of $0.37 \text{ cm}^3/\text{sec}$, $[HF] = 1.06 \times 10^{-8} \text{ mol/cm}^3$. The outgassing surface was 190 cm^2 . The forward direction of eq. (9) is favored, as seen in the equilibrium constant; $K(1200^\circ K) = 6.8 \times 10^{27}$ and $K(1500^\circ K) = 1.9 \times 10^{25}$ (unit: atm^2). Hence, since $[CF_4] \gg [H_2O]$ from outgas, we assumed 100% conversion of outgas H_2O to $2HF$. This assumption leads to an H_2O -outgas flux of $1.0 \times 10^{-11} \text{ mol/cm}^2/\text{sec}$, which agrees in magnitude with the observed outgassing of the Astro furnace.

Table 2 shows that the degree of conversion of H_2O to $2 HF$ increases with temperature but, at a given temperature, is inversely proportional to the ratio of $[H_2O]:[CF_4]$. Thus, at $900^\circ C$, 100% conversion is expected for $[H_2O]:[CF_4] = 1:10^3$. For the given dilution of 5 mol% CF_4 in He, it is seen that the conversion increases by a factor of 3.2 for a temperature increase of $100^\circ C$. Assuming a simple Arrhenius dependence of the rate on temperature, a value of $[H_2O]:[CF_4] = 1:10$ from 5 mol% CF_4 in He would be completely converted at temperatures equal to or greater than $1300^\circ C$. These results apply to a

residence time in the chamber of 500 sec, which is a factor of two to four smaller than the cases of crystal growth.

We conclude from these studies in fluoride RAP that

1. To provide rapid RAP of the condensed phase, HF should be the primary agent.
2. To lower the RAP index, CF_4 can be used to convert H_2O to 2HF . If the process temperature is low, e. g., 900°C , complete conversion can be approximated with $[\text{H}_2\text{O}]:[\text{CF}_4] = 1:10^3$. If the process temperature is high, e. g., 1300°C , then complete conversion is realized at $[\text{H}_2\text{O}]:[\text{CF}_4] = 1:10$.

TABLE 2. REACTION OF CF_4 WITH H_2O IN GRAPHITE

$\frac{[\text{H}_2\text{O}]}{[\text{CF}_4]} 10^{2a}$	$\frac{[\text{HF}]}{4[\text{CF}_4]} 10^2$		$\frac{[\text{HF}]}{2[\text{H}_2\text{O}]} 10^2$	
	900°C	1000°C	900°C	1000°C
(0.0)	0.13	—	(100)	(100)
2.6	0.06	0.13	4.3	9.6
12.0	0.05	0.17	0.85	2.8
55.0	0.05	0.16	0.19	0.59

^aThe value of (0.0) refers to H_2O from outgassing of the apparatus, 12 to saturation of the gas at 0°C , and 55 to saturation at 25°C . The gas was 5 mol% CF_4 in He. The value of 2.6 was obtained by saturation of pure CF_4 with H_2O at 25°C .

From the H_2O outgas in the Astro furnace, we estimate that the CF_4 mole fraction in the vapor phase should be $\approx 10^{-3}$. Two RAP recipes were compared in the crystal growth study: $[HF]:[HF]$ = 0.44:0.56 (RAP-1) and $[HF]:[He]:[CF_4]$ = 0.44:0.56:0.0028 (RAP-2). All Bridgman crystal ingots grown were 4.2 cm diameter.

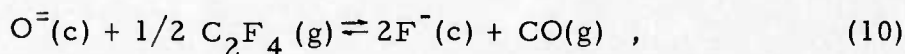
Since MF_2 was grown previously in RAP-1 we grew CaF_2 , SrF_2 , and BaF_2 by RAP-2. The infrared transmission of 5 cm path of these crystals (Beckman IR 12) showed improved transparency over their respective counterparts grown by RAP-1 in an earlier study.⁹ However, when the melt receives a longer soaking in RAP-1, the IR transparencies by RAP-1 and RAP-2 look the same. In this case, the higher sensitivity derived from optical calorimetry is needed to detect the smaller difference in the absorption coefficient, e.g., 0.1%/cm.

Melting congruency experiments under HF/He showed that Ca-Sr and Sr-Ba cation pairs produce homogeneous crystal specimens, but Mg-Ca and Ca-Ba do not. The published phase diagrams of MgF_2 - CaF_2 show a simple binary with one eutectic point.^{10,11} In CaF_2 - SrF_2 a continuous solid solution is reported with a shallow minimum near 50 mol% SrF_2 and 1330°C.¹² Similarly, in the case of SrF_2 - BaF_2 with the shallow minimum at 19 wt.% Sr.¹³

Single-crystal ingots of the minimum melting solid solutions, $Ca_{0.54}Sr_{0.46}F_2$ and $Sr_{0.34}Ba_{0.66}F_2$, were grown by RAP-1 and RAP-2. Figure 2 shows the typical size of pieces fabricated from the Bridgman ingot and the clarity as observed through the growth axis.

As detailed above, our approach to RAP growth is to use the fast-acting HF as the primary agent and provide minor amounts of a secondary agent, such as CF_4 , to achieve a low RAP-index. The RAP agent recommended by workers in the USSR is C_2F_4 , obtained from the depolymerization of $(C_2F_4)_n$ or Teflon (also called PTFE).¹⁴

Because $\Delta G^{\circ}(C_2F_4) > \Delta G^{\circ}(CF_4)$, where ΔG° is the free energy of formation, oxide conversion to the fluoride shows a larger lowering in free energy with the use of C_2F_4 ,



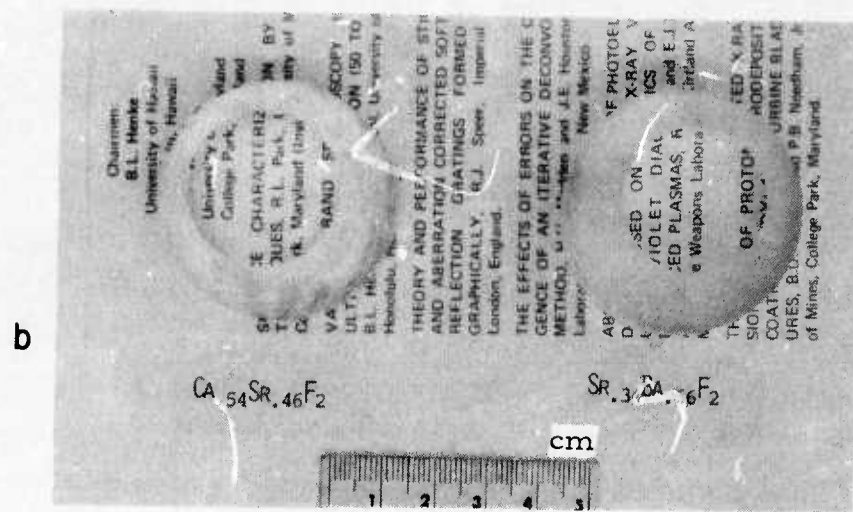
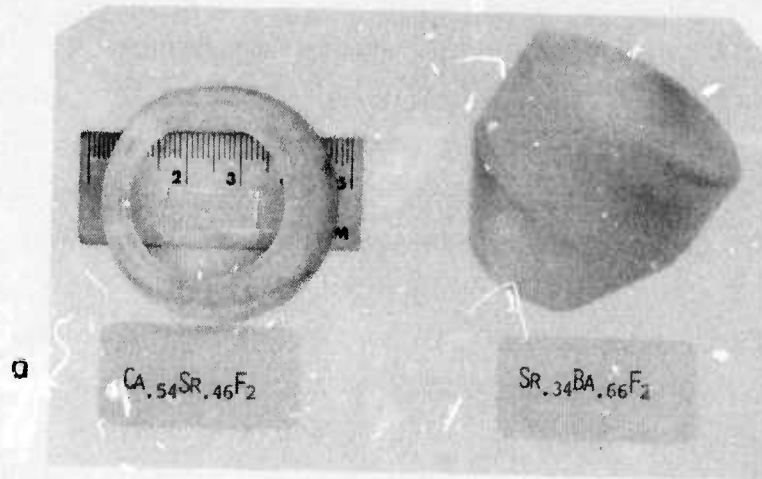
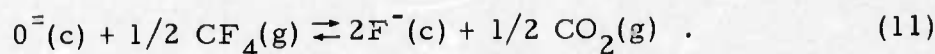


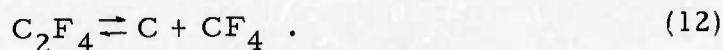
Figure 2. Single-crystal ingots of the minimum-melting solid solutions of the alkaline earth fluorides. (a) Typical size of the Bridgman ingots after fabrication. (b) Crystal clarity as observed along the growth axis.

and



Oxide conversion to fluoride is also more thermodynamically favored in CF_4 than in HF. However, we observe the reaction of CF_4 to $\text{O}^-(\text{c})$ at 800°C to be many orders of magnitude smaller than the reaction of HF to $\text{O}^-(\text{c})$ at 25°C . We expect very low reaction rates also in eq. (10). The C-F stretching mode absorbs strongly at $\nu = 4 \times 10^{13} \text{ sec}^{-1}$ (Ref. 5). From $D = 121 \text{ kcal}$ (Ref. 3), the specific rate constant of the $f = 0$ path of eq. (5) at 1430°C (CaF_2 mp) is $k \leq 0.04 \text{ sec}^{-1}$.

Comparison of eqs. (10) and (11) show that the free energy difference between the reactants is due to $\Delta G^\circ(\text{C}_2\text{F}_4) > \Delta G^\circ(\text{CF}_4)$, and between the products is due to $\Delta G^\circ(\text{CO}) < 1/2 \Delta G^\circ(\text{CO}_2)$. These two differences are tied to the combustion reaction of CO to CO_2 and to the dissociation,



Because $\Delta G^\circ(\text{C}_2\text{F}_4) > G^\circ(\text{CF}_4)$, the forward direction of eq. (12) is favored: $[\text{CF}_4]:[\text{C}_2\text{F}_4]$ is 10^{16} at 600°C and 10^6 at 1430°C (CaF_2 mp).

Kinetically, the forward direction of eq. (12) may be expected to have a realistic rate at temperatures well below the MgF_2 RAP working temperatures. From the bond strength and vibration frequency, the rupture probability for $-\text{C} = \text{C}-$ at 1430°C is greater than $1000\%/ \text{sec}$.

In the pressure range 0.2 to 1.0 mm Hg of $\text{P}(\text{C}_2\text{F}_4)$, decomposition occurred at 900°C on the surface of CaF_2 powder.¹⁵ Much lower values of $\text{P}(\text{C}_2\text{F}_4)$ must have been involved in the observation that decomposition did not occur until 1200°C .¹⁶

From our DTA characterization runs of PTFE we deduced that after complete depolymerization at 550°C , $(\text{C}_2\text{F}_4)_n \rightarrow n \text{C}_2\text{F}_4$, decomposition by eq. (12) at $\text{P}(\text{C}_2\text{F}_4) \approx 10 \text{ atm}$ occurred below 600°C . Using He as a carrier gas with an average value of $\text{P}(\text{C}_2\text{F}_4) = 40 \text{ mm}$, at a flow of $0.5 \text{ cm}^3/\text{sec}$, a 2 min residence time through the pyrolysis chamber (stainless steel coil) showed a GC elution spectra of $[\text{C}_2\text{F}_4]:[\text{CF}_4] \approx 1:10^3$.

We therefore consider PTFE as an inexpensive source of high-purity CF_4 , an expensive RAP agent. However, the breakdown shown in eq. (12) must be avoided in the growth apparatus because of the tendency of the carbon deposit to form a stable suspension in the fluoride melt. This study consisted of two phases:

1. Depolymerization kinetics of PTFE for the generation of C_2F_4
2. Production of CF_4 from C_2F_4

In support of the first phase, we carried out first DTA (thermal) characterization of the breakdown of PTFE. Our DTA thermogram measurements (DuPont 900 Thermal Analyzer) show two endotherms in the heat-up of PTFE. The first endotherm corresponds to a reversible process. It is a small peak which begins at 321°C and corresponds to the melting point.^{17,18} The second endotherm corresponds to an irreversible process, $(\text{C}_2\text{F}_4)_n \rightarrow n \text{C}_2\text{F}_4$. It is a large peak that begins at 550°C .

The next thermal characterization of virgin PTFE powder was a series of isothermal runs under various atmospheres. The depolymerization rate was studied from 470 to 545°C using the DuPont 900 Thermal Analyzer thermogravimetric analysis (TGA) module. The weight (W) of PTFE decayed with time (t) as a first-order process in vacuum, Ar, CO_2 , or O_2 . At each temperature setting, the decay was followed over a time interval greater than, or equal to, the half-life. In these four cases, the linear fit to $\ln W$ versus t , by the method of least squares, yielded a correlation coefficient with a deviation of 0.1%, from unity.

Although a first-order decay in W at various temperature settings was obtained for each atmosphere, the plot of $\ln k$ versus reciprocal temperature was not linear in the range 470 to 550°C . This is seen in Fig. 3. Our results in vacuum agree with the reported energy barrier of 83 kcal/mol in the range 360 to 510°C .¹⁹ Yet, at temperatures greater than 530°C , it appears that the degradation path in vacuum has a lower barrier.

Only at pressures less than 5 mm does thermal degradation (600°C) of PTFE yield 100% monomer (C_2F_4); at one atmosphere, the

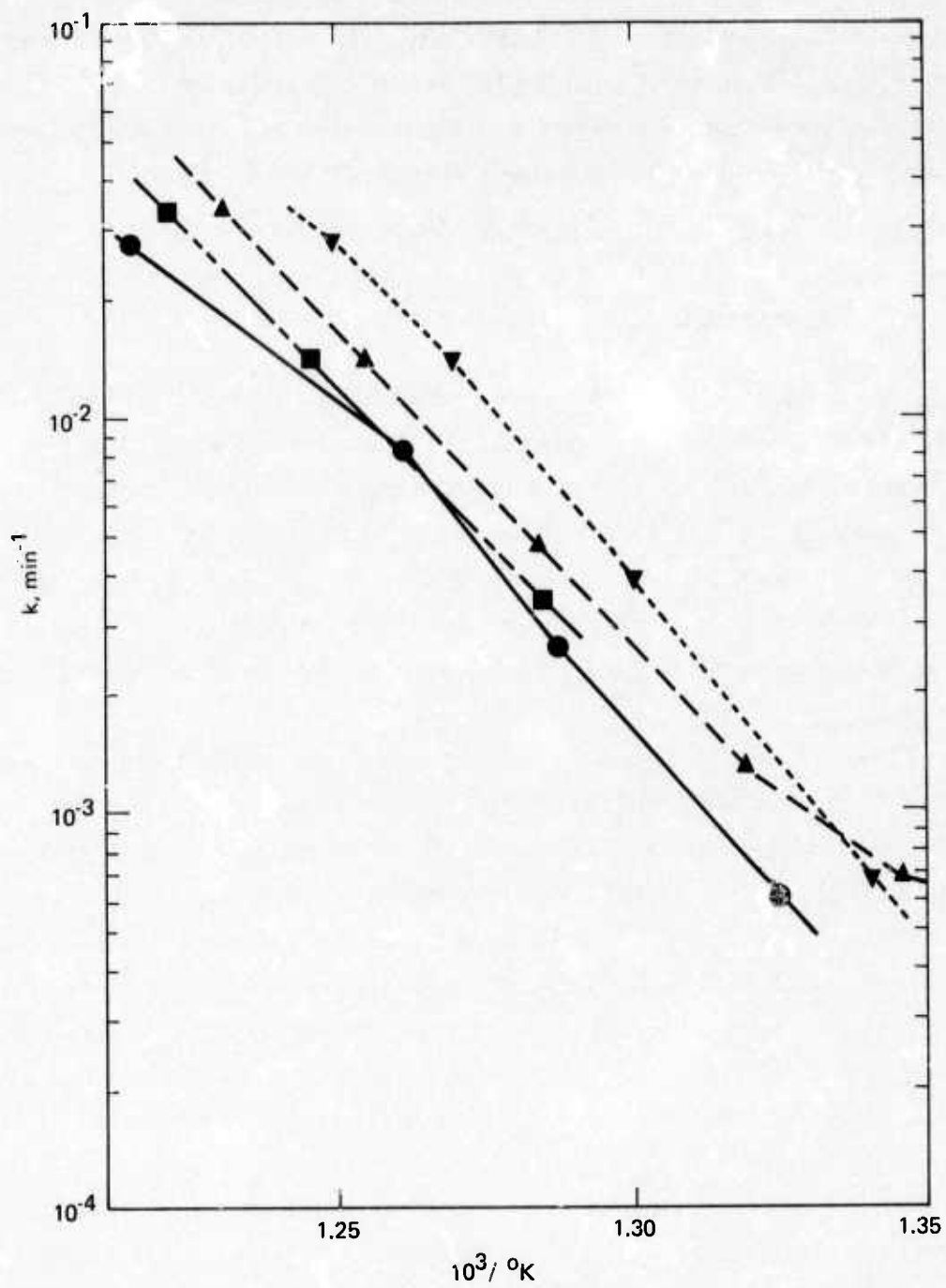


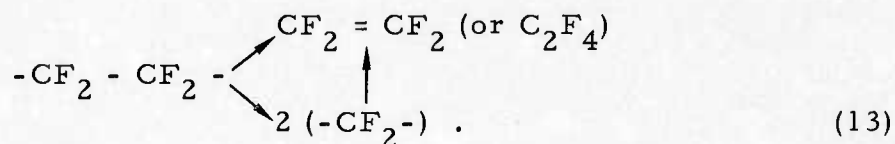
Figure 3. Temperature dependence of the decay constant (k) for the depolymerization of TFE under various atmospheres: ●, vacuum; ■, Ar; ▲, CO_2 ; and ▼, O_2 .

products are C_2F_4 (16%), C_3F_6 (26%), and C_4F_8 (58%).²⁰ The product variations are believed to be caused by reactions between C_2F_4 and the radical $-CF_2-$.

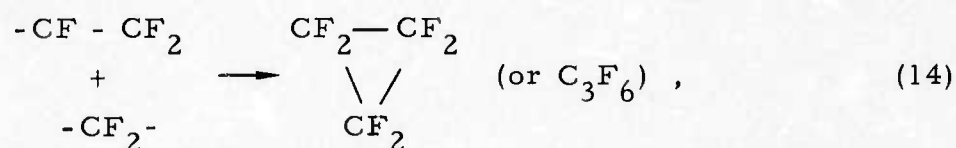
Surface degradation of the solid by the radical is in harmony with the following observations:

1. Linear dependence of $\ln W$ on time
2. Change in energy barrier with temperature (Fig. 3)
3. Slight effect of the nature of the atmosphere on 2 (Fig. 3).
4. Formation of C_2F_4 , C_3F_6 , and C_4F_8 in the vapor phase.

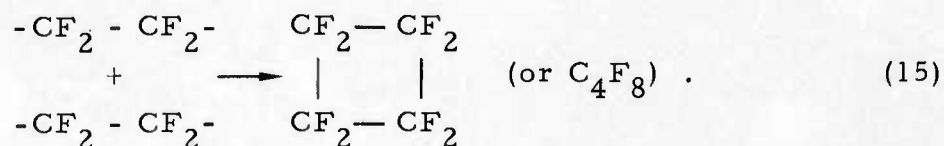
The C-C bond is much weaker than the C-F bond. Hence, the first observation indicates that the removal of units of $-CF_2-$ and $-CF_2-CF_2-$ occur at some energy barrier. There are two paths possible for the latter species in the vapor phase,



As vapor phase concentrations build up, side reactions follow,



and



Now, a $-CF_2-$ reacting with another $-CF_2-$ is already taken care of in eq. (13). All these vapor phase reactions explain observation 4, but do not affect the energy barrier for thermal degradation of the solid. However, a $-CF_2-$ attacking the surface to pull out a $-CF_2-CF_2-$ will lower the energy barrier and provide a basis for observations 2 and 3.

The second phase of this study, i. e. , the production of CF_4 from C_2F_4 , still remains to be done.

IV. EVALUATION

Task A: Bromide (KBr)

Two RAP agents, CH_2Br_2 and CF_3Br , were employed in the growth of KBr, with He as the carrier gas. The mixture $\text{CF}_3\text{Br}/\text{He}$ was more effective than $\text{CH}_2\text{Br}_2/\text{He}$ for scrubbing the KBr melt but was also more corrosive to the crucible (SiO_2). Measurements with the Beckman IR 12 showed that KBr crystals grown in $\text{CH}_2\text{Br}_2/\text{He}$ invariably yield a flat transmission from 2.5 to 18 μm (Fig. 4 (a)). Those grown in $\text{CF}_3\text{Br}/\text{He}$ show extraneous absorption bands which vary from one run to the next (Fig. 4(b)).

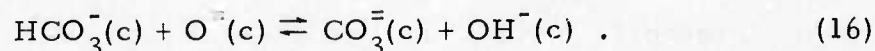
These variable absorptions probably were caused by impurities leached out during corrosion of the crucible. However, the extraneous band at 13 μm was always present with an absorption coefficient on the order of 1%/cm. This band could be caused by F^- impurity arising from the interaction of CF_3Br with the crucible (SiO_2). The extraneous bands arising from the use of $\text{CF}_3\text{Br}/\text{He}$ were removed by $\text{CH}_2\text{Br}_2/\text{He}$, as shown in Fig. 4(c).

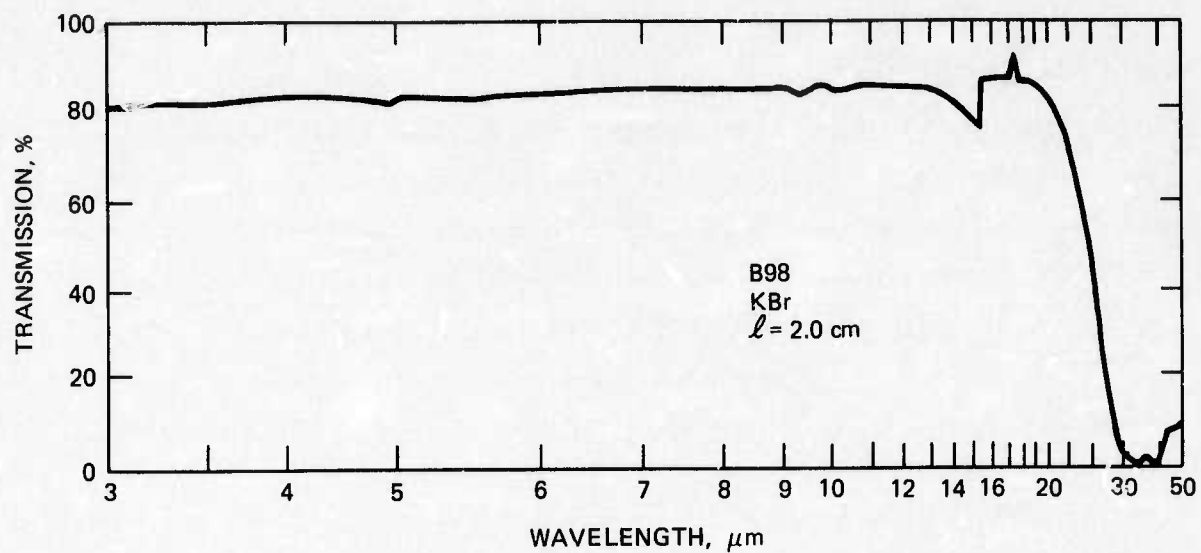
Bulk and surface absorptions at 10.6 μm of KBr grown in $\text{CF}_3\text{Br}/\text{He}$ and $\text{CH}_2\text{Br}_2/\text{He}$ were measured. The results are discussed in Task B and summarized in Table 3.

Task B: Chloride (KCl)

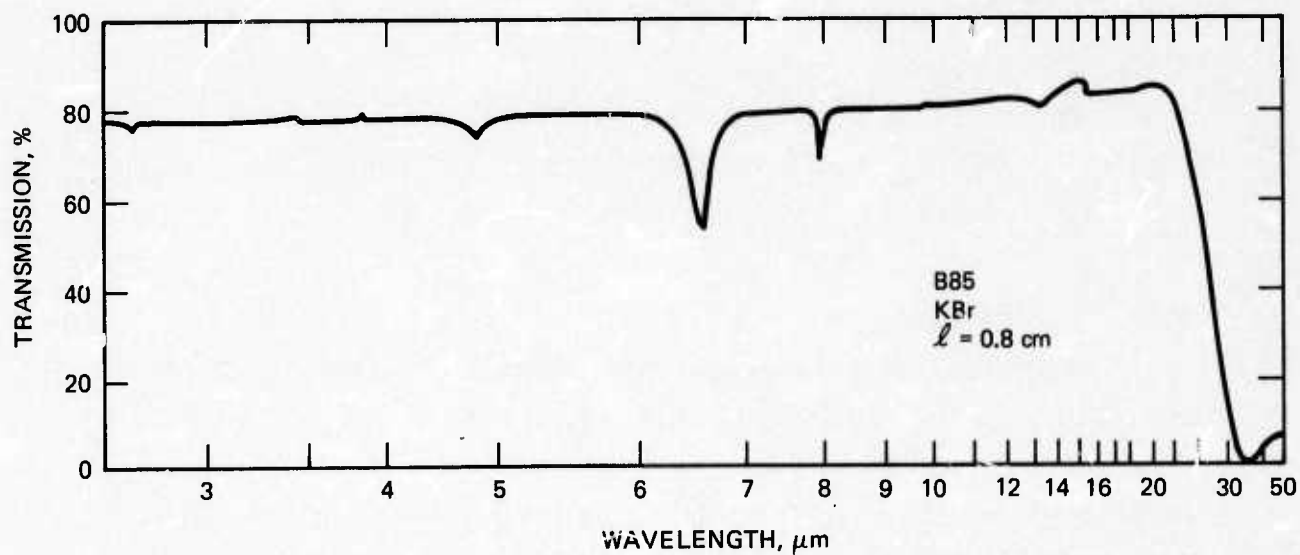
Numerous oxyanion impurities contribute to the optical absorption at 10.6 μm .¹ The anion impurities that are of particular concern to RAP growth of KCl in $\text{CCl}_4/(\text{He}, \text{CO}_2)$ are the carbonate ($\text{CO}_3^{=}$) and the bicarbonate (HCO_3^-). The reactions leading to the formation of these anions were discussed in Section III.

The bicarbonate/carbonate ratio is linked to the hydroxide/oxide ratio,



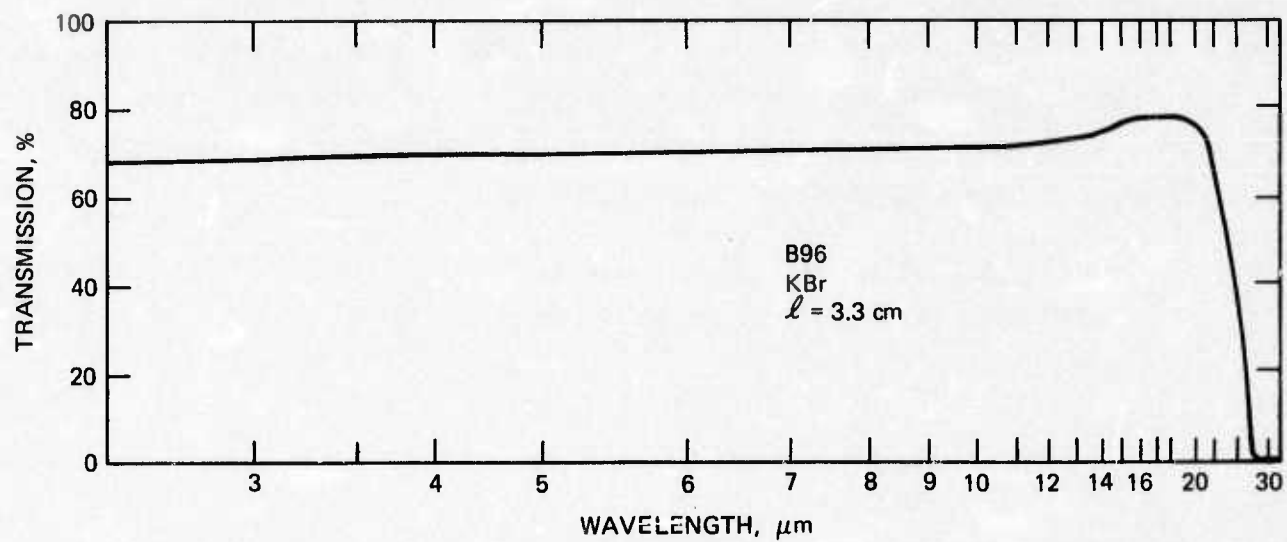


a RAP grown in $\text{CH}_2\text{Br}_2/\text{He}$.



b RAP grown in $\text{CF}_3\text{Br}/\text{He}$.

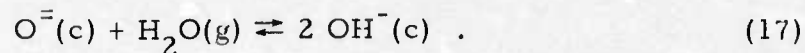
Figure 4. Infrared transmission of KBr single crystals.



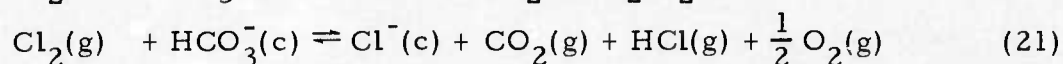
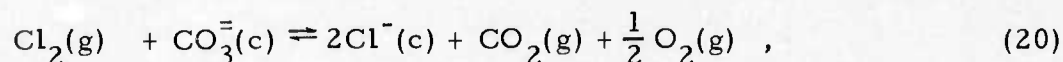
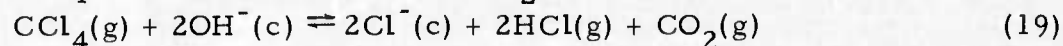
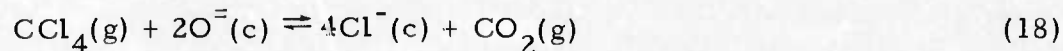
c Melt soaked initially in $\text{CF}_3\text{Br}/\text{He}$ and finally in $\text{CH}_2\text{Br}/\text{He}$.

Figure 4. Continued.

These anion impurities are subject to RAP because the hydroxide/oxide ratio depends on the presence of H_2O ,



The preceding reactions illustrate the gettering effect of CO_3^{2-} and HCO_3^{-} , through the lowering of the RAP index of the vapor phase. Displacement reactions are also effected in the condensed phase by the RAP agent, or its pyrolysis product, Cl_2 :



Since these reactions are thermodynamically favored, it was expected that the incorporation of CO_3^{2-} and HCO_3^{-} would be insignificant in RAP with $CCl_4/(He, CO_2)$. This expectation was realized. Measurements with the Beckman IR 12 showed an infrared transparency in KCl grown in CCl_4/CO_2 similar to that grown in CCl_4/He . An example is shown in Fig. 5.

We attempted to separate the bulk (β) and surface (σ) contributions to the total absorption (α) at 10.6 μm . We hoped to correlate the value of β to crystal quality and σ to the quality of the surface finish. The method described by M. Hass²¹ was used with samples of RAP KCl and KBr where the length: diameter ratio was equal to or greater than 7. The results are presented in Table 3.

Some of the inconsistencies in the data can be attributed to the presence of scattering centers in the bulk. Boules KBr-B72B, KCl-B129 and KCl-B62 A and B were examined with a 6328 \AA He-Ne laser beam along the cylindrical (growth) axis. The sides of the fabricated prisms were polished to allow observation of scattering perpendicular to the beam.

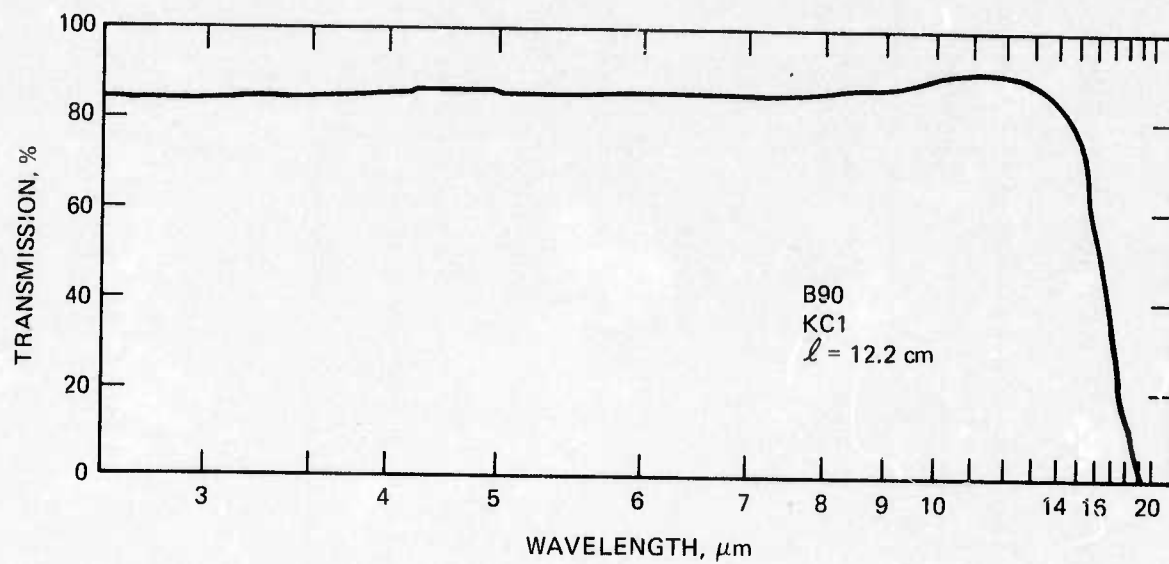


Figure 5. Infrared transmission of a 12.2 cm long KCl single-crystal ingot (3 cm diameter) grown in CCl_4/CO_2 .

TABLE 3. BULK AND SURFACE ABSORPTIONS AT 10.6 μm OF KCl AND KBr SINGLE CRYSTALS

Boule No.	RAP ^a Agent	Length, cm	Width, cm	β , cm^{-1}	σ , %/Surface		Comments
					Polished	Etched	
KCl-B62A	CCl_4	13.5	2.1	7.1×10^{-5}	0.21	0.010	Right-tetragonal prisms cut from the same boule and with the sides polished.
KCl-B62B	CCl_4	13.5	2.1	5.0×10^{-5}	—	0.030	
KCl-B129	CCl_4	17.6	2.5	1×10^{-4}	—	0.040	
KBr-B72B	CH_2Br_2	8.5	1.7	7×10^{-5}	—	—	β not reproducible. Probably due to scattering centers.
KBr-B88A	CF_3Br	10.0	1.7	8×10^{-4}	0.35	—	Right-tetragonal prism with the sides polished
KBr-B102	CH_2Br_2	4.0	4.0	—	—	—	$a = 2.2 \times 10^{-4} \text{ cm}^{-1}$, polished. $a = 2.0 \times 10^{-4} \text{ cm}^{-1}$, etched.

^aThe carrier gas was He.

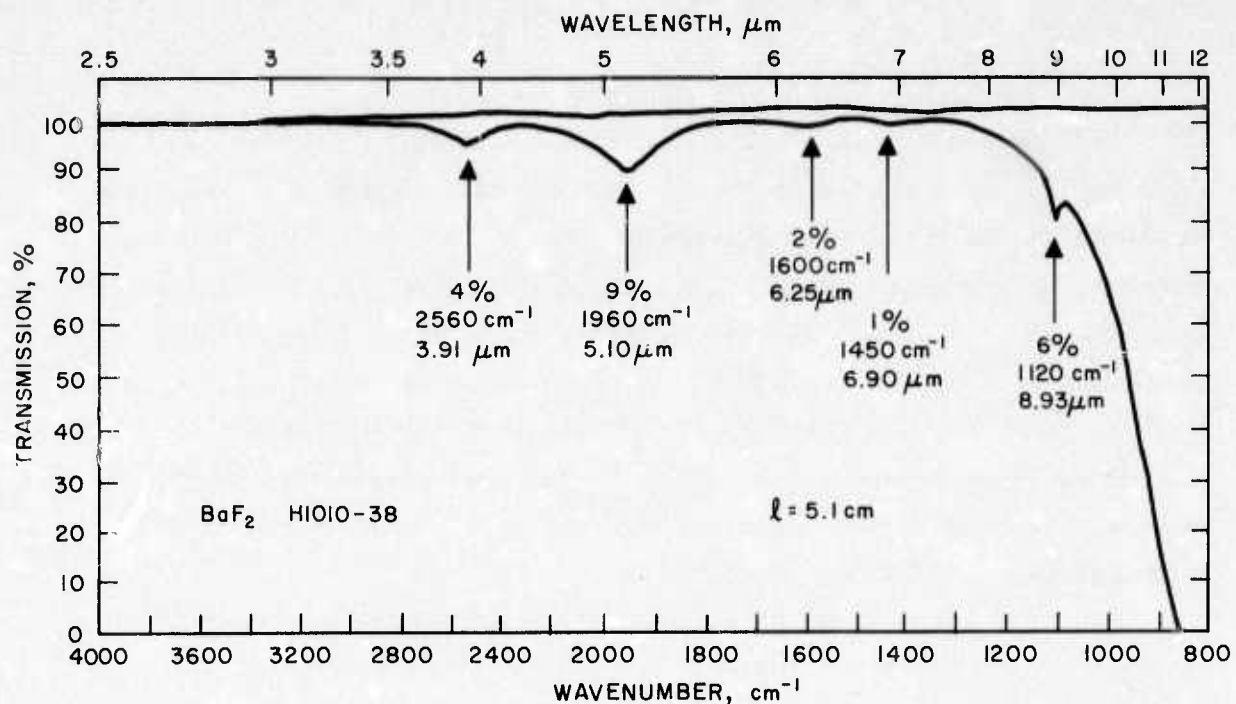
In KBr-B72B and KCl-B129, small scattering centers were observed in the last inch of growth. On the other hand, KCl-B62A and B showed no such scattering perpendicular to the beam but a diffuse forward scattering at small angles to the He-Ne beam. The latter type of scattering was also observed in the other boules. We suspect that the irreproducible value of β (Table 3), large absorption ($\alpha = 3 \times 10^{-4} \text{ cm}^{-1}$), and abnormal heating and cooling curves in KBr-B72B stem from these scattering centers. It should also be noted that β in KCl-B129, where scattering centers were observed, is higher than that in B62A and B (diffuse scattering only).

The value of β for RAP KBr is undoubtedly below the value of α obtained for a thin sample (KBr-B102) as listed in the last column of Table 3. The value obtained from the initial runs on KBr-B72B, where presumably, a greater fraction of the scattering centers were fortuitously avoided, is probably the best estimate of β for the first generation of RAP KBr boules.

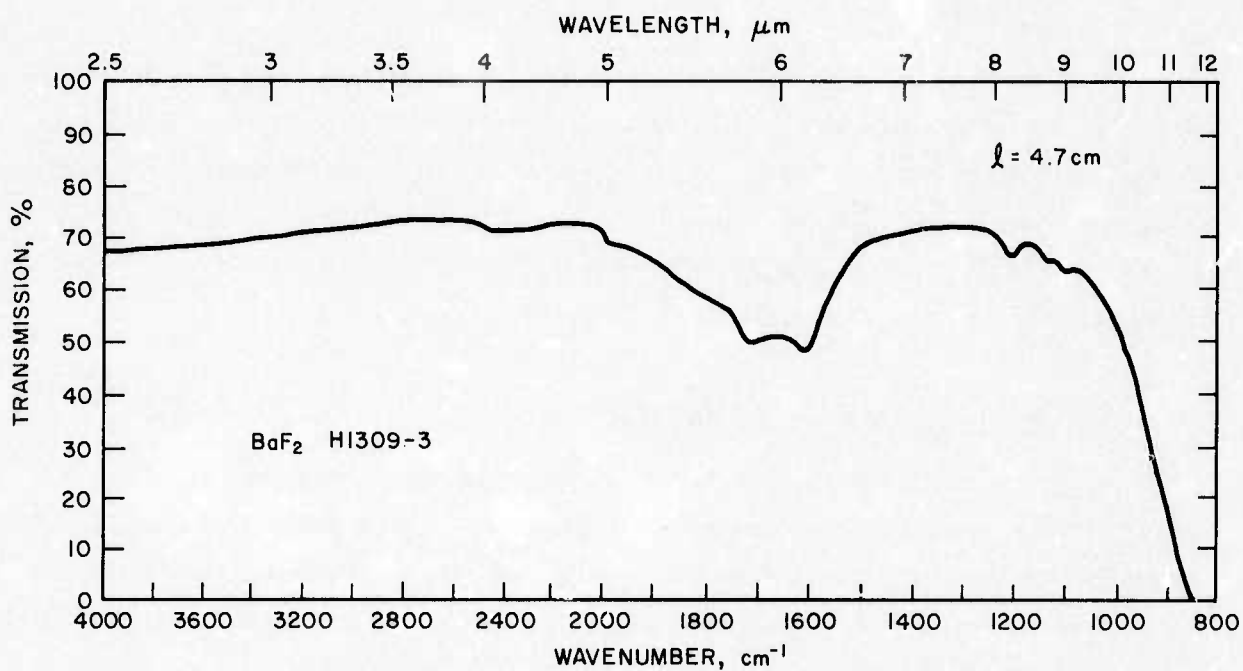
The effectiveness of the etch procedure developed for KCl is seen in the values of σ for KCl-B62A, before and after etching. These results are consistent with numerous measurements on various RAP KCl window samples, before and after etching. However, an analogous etch procedure for KBr (using HBr instead of HCl solution) did not significantly improve the value of σ .

Task C: Fluoride (MF_2 and Solid Solutions)

Extraneous absorption bands in the infrared, from undefined anion impurities, are not removed by processing and growth of BaF_2 , at its melting point, in HF/He. These bands show no correlation with the anion purity of the source material, as seen in Figs. 6(a) and (b). However, the displacement reaction by the RAP agent (HF) becomes effective if the BaF_2 melt is processed at the melting temperature of CaF_2 (200°C above the melting point of BaF_2). This result is shown in Fig. 6(c). The soaking period of the melt may be shortened if a secondary RAP agent is used to lower the RAP index. Figure 6(d) gives the spectrum of single crystal BaF_2 grown in (HF, CF_4) He. (The molar ratios are given in Section III).

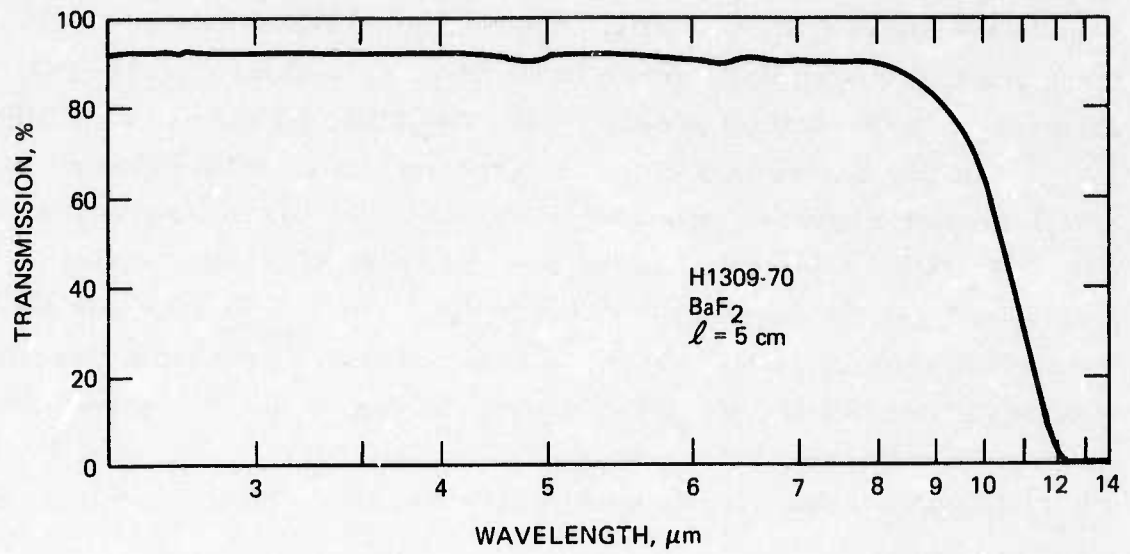


a Crystal grown from five-nines pure BaF₂ powder.

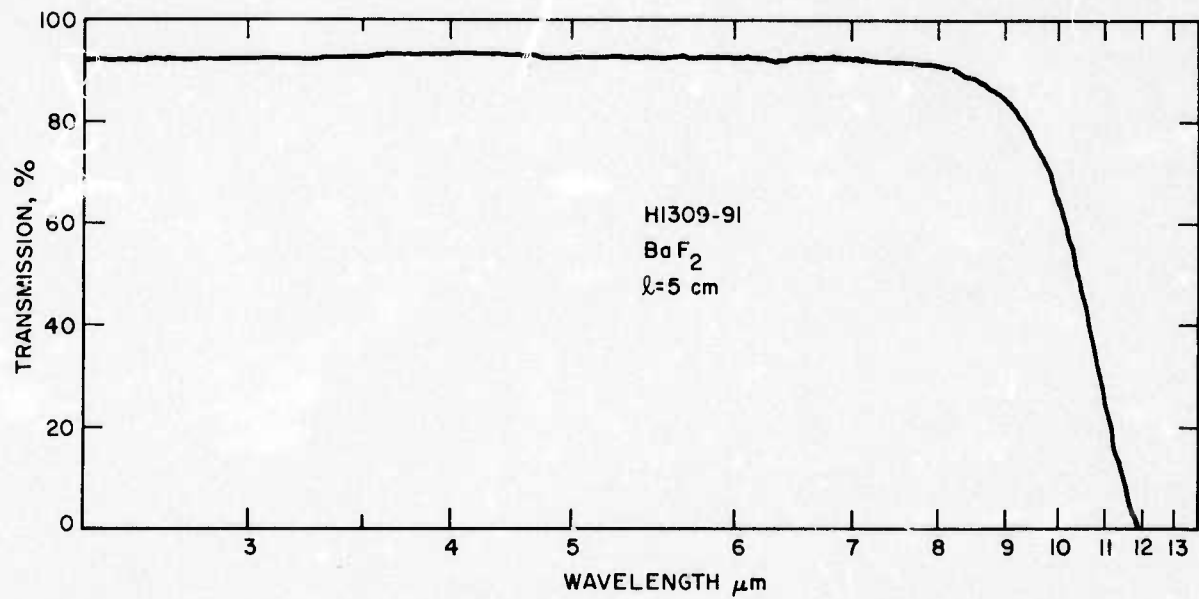


b Crystal grown from BaF₂ powder converted from five-nines pure BaCO₃.

Figure 6. Infrared spectrum of single crystal BaF₂ grown in HF/He.



c Same material as in a with the addition of a one hour soak of the melt in HF/He at $\sim 200^{\circ}\text{C}$ above the melting point of BaF₂.

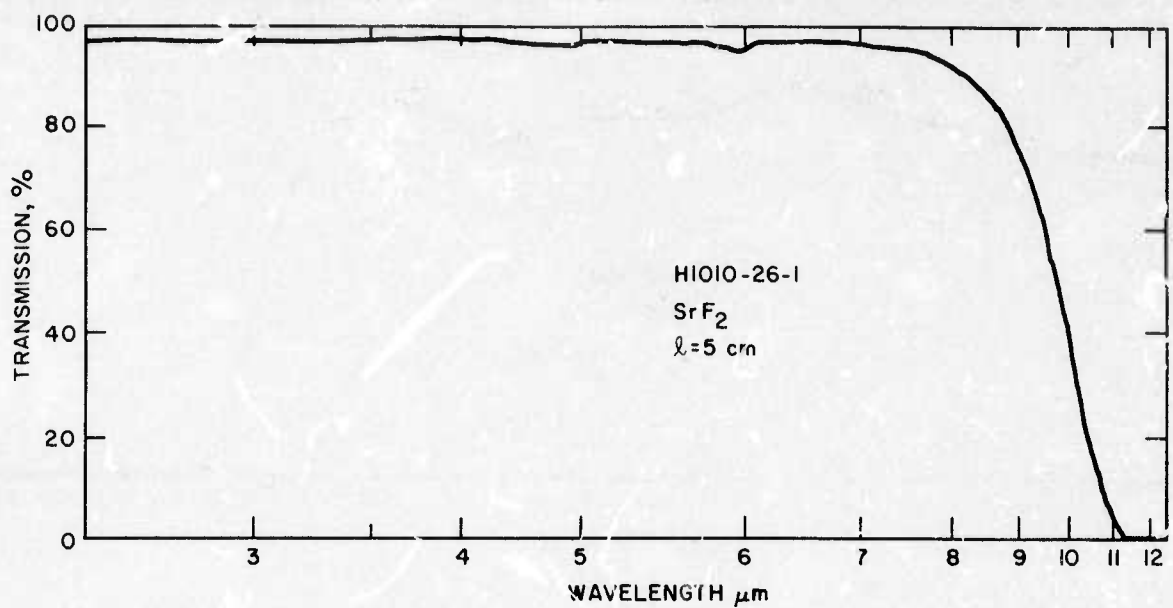


d Same as in c with less than one hour soak of melt in (HF, CF₄)/He.

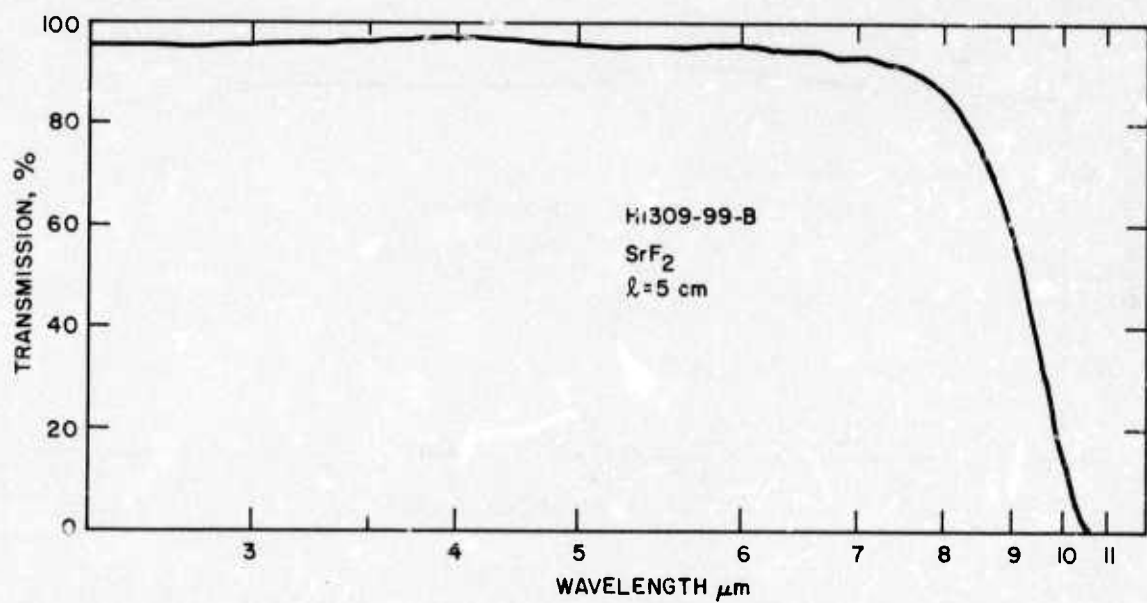
Figure 6. Continued.

A similar improvement in the infrared transmission of SrF_2 is seen in the use of $(\text{HF}, \text{CF}_4)/\text{He}$. Figure 7(a) shows an absorption in the $6 \mu\text{m}$ region with SrF_2 grown in HF/He . This absorption band is not present in the crystal grown in $(\text{HF}, \text{CF}_4)/\text{He}$, as seen in Fig. 7(b).

Similar differences in the infrared spectra of solid solutions of alkaline-earth fluorides were also observed in the use of HF/He and $(\text{HF}, \text{CF}_4)/\text{He}$. Figure 8(a) shows a broad absorption band, extending from 6 to $7 \mu\text{m}$, in the single-crystal of $\text{Sr}_{0.34}\text{Ba}_{0.66}\text{F}_2$ grown in HF/He . This broad absorption was absent when the crystal of the same composition was grown in $(\text{HF}, \text{CF}_4)/\text{He}$, as seen in Fig. 8(b). The growth of these solid solutions, $\text{Sr}_{0.34}\text{Ba}_{0.66}\text{F}_2$ and $\text{Ca}_{0.54}\text{Sr}_{0.46}\text{F}_2$, in $(\text{HF}, \text{CF}_4)/\text{He}$ yields single crystals which are transparent from 2.5 to $6 \mu\text{m}$, as shown in Figs. 8(b) and (c).

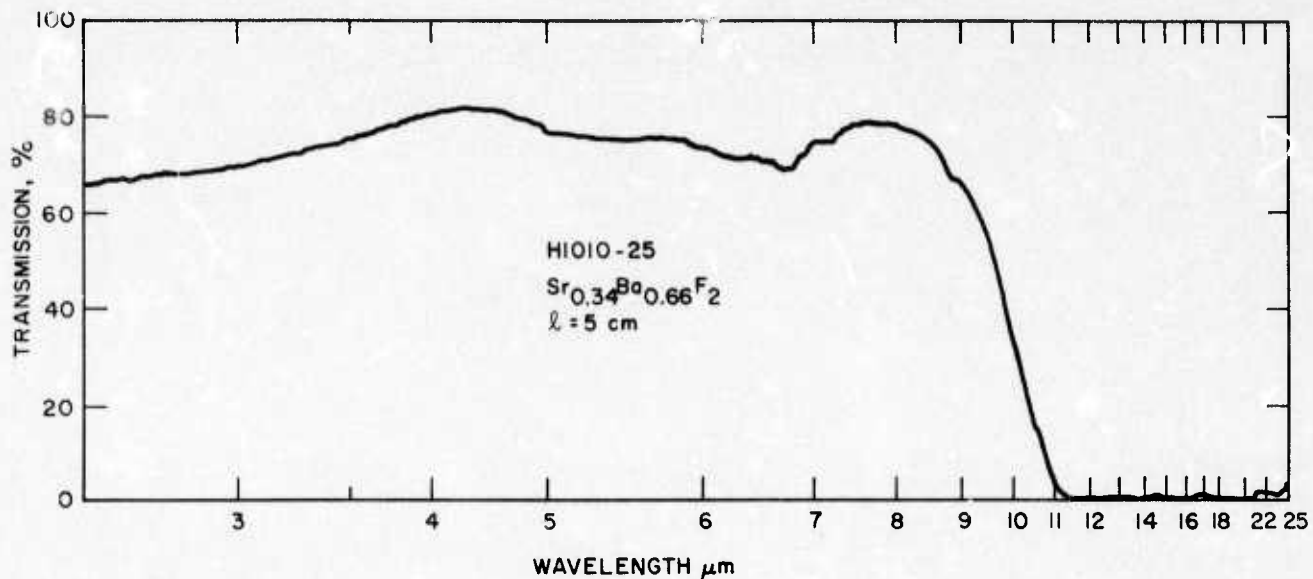


a Single crystal SrF₂ grown in HF/He.

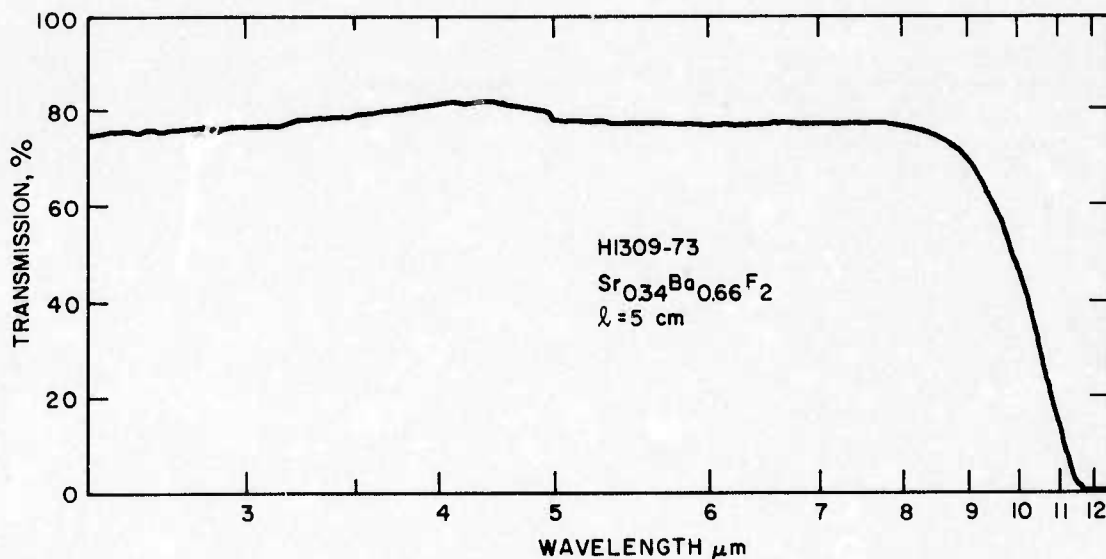


b Single crystal SrF₂ grown in (HF, CF₄)/He.

Figure 7. Infrared spectrum of single crystal SrF₂.

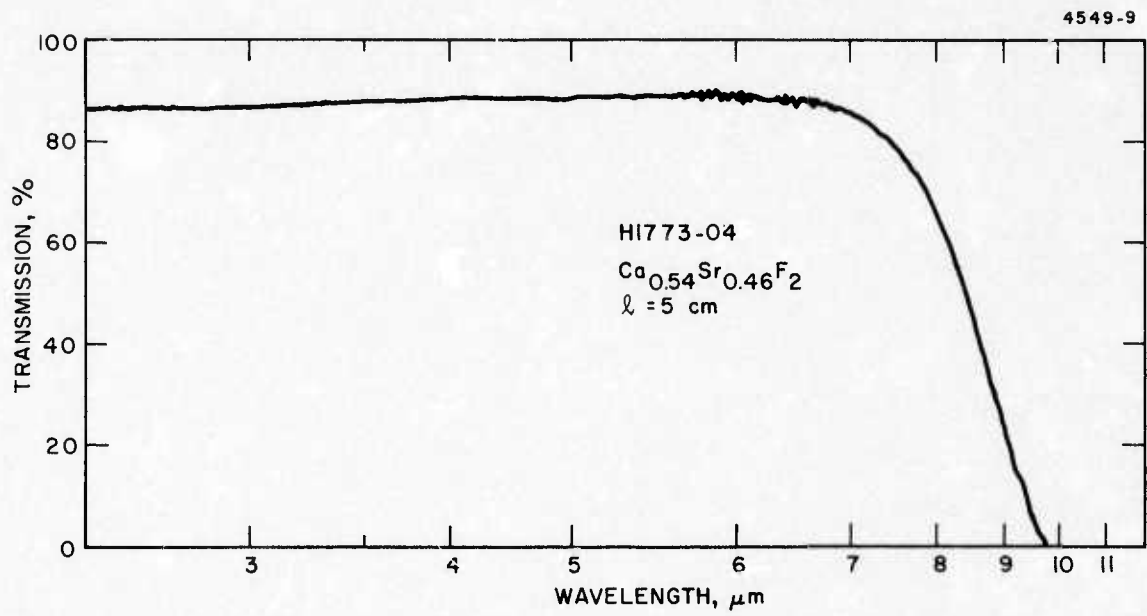


a Single crystal $\text{Sr}_{0.34}\text{Ba}_{0.66}\text{F}_2$ grown in HF/He.



b Single crystal $\text{Sr}_{0.34}\text{Ba}_{0.66}\text{F}_2$ grown in $(\text{HF}, \text{CF}_4)/\text{He}$.

Figure 8. Infrared spectra of single-crystal, minimum-melting, solid solutions of the alkaline-earth fluorides.



c Single crystal $\text{Ca}_{0.54}\text{Sr}_{0.46}\text{F}_2$ grown in $(\text{HF}, \text{CF}_4)/\text{He}$.

Figure 8. Continued.

V. CONCLUSIONS AND RECOMMENDATIONS

The use of $\text{CH}_2\text{Br}_2/\text{He}$ in the growth of KBr has yielded consistently a value of $\alpha = 2 \times 10^{-4} \text{ cm}^{-1}$, the absorption coefficient at $10.6 \mu\text{m}$. While this is an order-of-magnitude improvement in α over non-RAP KBr, we know that the present situation is still not the optimum. Only in one calorimetry run did we obtain $\alpha = 2 \times 10^{-5} \text{ cm}^{-1}$.

The insufficient removal of OH^- (c) and its derivative anions is indicated in all runs by partial sticking of the crystal ingot to the crucible (silica). These KBr specimens still show sensitivity to the environment (fogging). Consequently, we recommend that the RAP chemistry study continue, with the objective of achieving a more efficient removal of OH^- (c).

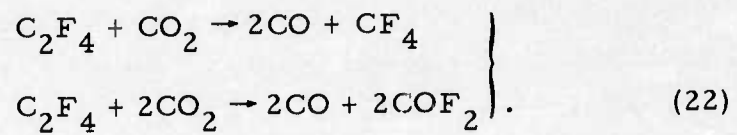
Reactive atmosphere process growth of 4 cm diameter KCl now yields consistently 1.2 to $1.4 \times 10^{-4} \text{ cm}^{-1}$ as the measured total absorption. By the M. Hass method,²¹ the bulk absorption coefficient ranges from 6 to $9 \times 10^{-5} \text{ cm}^{-1}$.

The use of CO_2 gas in the carrier prevents deposition of carbon in the crystal and the CO_2 laser damage threshold measurements indicate a low content of inclusions. However, the problem of bubble formation must be controlled to achieve a reproducible RAP applicable to scale up. We recommend that this problem and the use of a lower $[\text{CCl}_4]:[\text{He}]$ ratio, to obtain a low f value, be studied.

The use of HF/He in the growth of MF_2 and its solid solutions has yielded crystal specimens with very high transparencies in the infrared. Further improvement was achieved by adding a small concentration of CF_4 , an agent which lowers the RAP index. To determine the optimum composition of the RAP gas, further study is needed to understand the H_2O -outgas flux during crystal growth and the efficiency of the CF_4 reaction with H_2O at the same temperature.

We showed that even in the case of C_2F_4 , a RAP agent favored by USSR workers, the action stems from the breakdown into CF_4 . Since Teflon is an inexpensive, high-purity source of C_2F_4 and CF_4 is

expensive, we recommend that a study to generate CF_4 from C_2F_4 be carried out. The study should also include the use of reactive carriers which offer the potential of yielding good RAP agents. For example, with CO_2 :



APPENDIX A

CRYSTAL GROWTH IN A REACTIVE ATMOSPHERE*

R. C. Pastor and A. C. Pastor
Hughes Research Laboratories
Malibu, California 90265

(Received November 15, 1974; Communicated by R. A. Huggins)

ABSTRACT

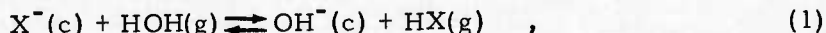
Concepts of reactive atmosphere processing (RAP) are applied to crystal growth. Steady state pyrolysis of CBr_4 shows the material to be applicable to RAP growth at $<600^\circ\text{C}$ and, therefore, inapplicable to the growth of KBr (mp = 730°C). Steady state pyrolysis of CCl_4 shows the material to be applicable to RAP growth up to 900°C and, therefore, useful to metal chlorides in general.

Introduction

The use of metal halides as windows for high power lasers at 2 to 6 μm and 10.6 μm requires rigid constraints on anion purity. The current practice to specify purity with respect to the cation is relevant to optical transmission at much shorter wavelengths from visible to ultraviolet. The vibrational modes of anions are infrared active and often involve high absorption cross sections so that much less than 1 ppm is needed to achieve absorption coefficients below 0.001 cm^{-1} in the crystal (1).

Reactive atmosphere processing (RAP) decomposes anions, e.g., OH^- , NH_2^- , NO_3^- , NO_2^- , HCO_3^- , CO_3^{2-} , $\text{C}_2\text{O}_4^{2-}$, etc., and quantitatively substitutes the halide.** Of these anions, OH^- poses a special problem because H_2O , its source, is ubiquitous. The oxygen-hydrogen vibration is active at 2 to 4 μm and the oxygen-cation vibration is active at 9 to 10 μm . At room temperature, a freshly generated surface of NaCl readily hydrolyzes (2). The OH radical is a pseudo-halogen with an electronegativity value between F and Cl , and OH^- is slightly larger in size than F^- (3).

The heterogeneous reaction (hydrolysis) in crystal growth is



*The work with CCl_4 and KCl was supported in part by ARPA Order No. 1256, Contract F29601-71-C-0101, and monitored by the Air Force Weapons Laboratory, Kirtland Air Force Base (New Mexico). The work with CBr_4 and KBr was supported in part by ARPA Order No. 2612, Contract F33615-74-C-5115, and monitored by the Air Force Materials Laboratory, Wright-Patterson Air Force Base (Ohio).

**To be presented in a separate publication.

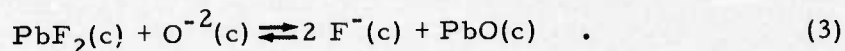
where X^- represents a halide, (c) a condensed phase (crystal and/or melt), and (g) the gas phase. The relation of concentrations in the condensed phase to the sources in the gas phase is,

$$C = \frac{[OH^-]}{[X^-]} = K \frac{P(H_2O)}{P(HX)} \quad (2)$$

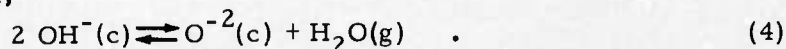
where K , the equilibrium constant of eq. (1), is fixed in the crystal growth of a material at its melting point. To achieve a low C , the RAP-index, $P(H_2O)/P(HX)$, must be low.

According to eq. (2), congruent growth with the gas phase based on the provision of a vacuum or an inert gas is characterized by a poor RAP-index, i.e., a high value. While the provision of halogen-hydride (HX) in the gas phase is an improvement, the RAP-index is limited by H_2O sources: the HX gas, moisture content of the charge and the outgas, corrosion action of HX on oxide surfaces, etc. These procedures focus solely on the manipulation of the gas phase.

Other procedures focus only on the condensed phase, e.g., the scavenging of O^{2-} in CaF_2 melt by PbF_2 (Ref. 4),

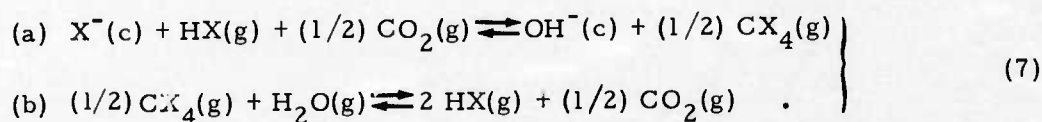
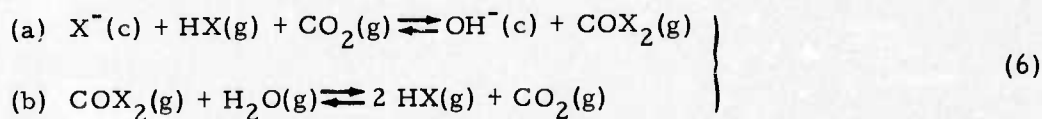
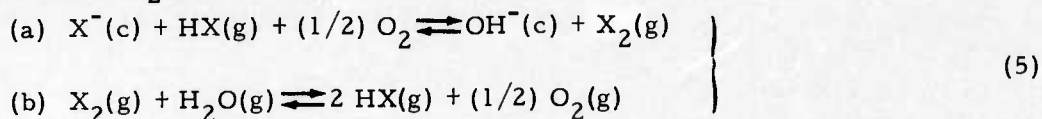


Excess PbF_2 and PbO are volatilized. Residual amounts of the scavenger throttle the growth rate. Also, the effectiveness of scavenging is subject to the RAP-index because,



If the RAP-index is high, it can be shown from eqs. (1), (3), and (4) that the net effect is the hydrolysis of PbF_2 in the CaF_2 melt by $H_2O(g)$.

An effective RAP procedure provides both paths for scavenging $OH^-(c)$ and $H_2O(g)$ at rates faster than provided by the sources. Thus, eq. (1) is represented as the sum of two partial reactions. For instance the equivalent of RAP with $X_2(g)$, $COX_2(g)$ and $CX_4(g)$ is as follows:



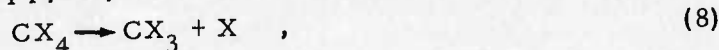
Note that the partial reaction (b) of each reaction couple of eqs. (5), (6), and (7) throttles the RAP-index since two moles of HX are formed at the expense of one mole of H_2O . RAP with X_2 , eq. (5(b)), is most effective only for $X_2 = F_2$. With $X_2 = Cl_2$, RAP begins to be effective at $>700^\circ C$ where chlorine becomes more oxidizing than oxygen. But with $X_2 = Br_2$, this cross-over is at a temperature much above the melting point of metal bromides, and in $X_2 = I_2$, the reaction is displaced even farther to the left.

Table 1 is a comparison of the three RAP procedures for chlorides, i.e., eqs. (5b), (6b), and (7b). The thermodynamic value of the RAP-index is calculated for the case where the source is at 0.1 atm and the initial value of $P(\text{H}_2\text{O}) = 10^{-4}$ atm.* It is seen that Cl_2 is the poorest RAP agent of the three. In KCl growth (mp = 1049°K), the RAP-index of Cl_2 is approximately the equivalent of HCl with a dewpoint (-60°C) considerably above its boiling point (-85°C).

TABLE 1
RAP-Index For Chlorides From 600° to 1200°K

T, $^\circ\text{K}$	Cl_2 RAP	COCl_2 RAP	CCl_4 RAP
600	0.51×10^{-3}	0.47×10^{-22}	1.2×10^{-20}
800	0.55×10^{-4}	1.4×10^{-20}	0.83×10^{-18}
1000	1.3×10^{-5}	0.43×10^{-18}	1.1×10^{-17}
1200	0.56×10^{-5}	0.43×10^{-17}	0.62×10^{-16}

The use of CCl_4 is preferred over that of COCl_2 because of toxicity and ease of handling. Now, CX_4 pyrolyzes to yield nascent X (Ref. 5),



which presents the possibility of chain propagation,



Termination reactions yield more C_2X_6 and X_2 ,

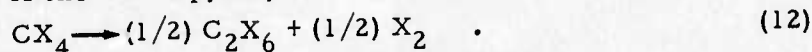


The advantage to having X is in the electron-transfer reaction,

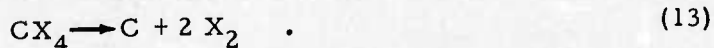


where the free energy change for the forward displacement, in the gas phase, is favorable for all X (Ref. 6): $\text{X} = \text{F}$, -42.7 ; $\text{X} = \text{Cl}$, -48.0 ; $\text{X} = \text{Br}$, -41.7 ; and $\text{X} = \text{I}$, -36.0 (unit: kcal/mole). The $\text{OH}^-(\text{c})$ need not diffuse out to the gas phase-condensed phase interface as a resonance transfer between $\text{X}^-(\text{c})$ and X at the interface brings $\text{X}(\text{c})$ in the proximity of $\text{OH}^-(\text{c})$.

The net reaction of the above pyrolysis is

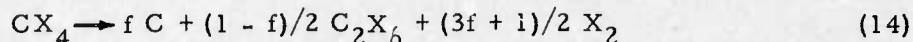


Unfortunately, there is another competing path in pyrolysis,



*The equilibrium constants as a function of temperature were obtained from, "Thermodynamic Properties of 65 Elements - Their Oxides, Halides, Carbides, and Nitrides," by C.E. Wicks and F.E. Block, Bull. 605 of the Bureau of Mines (U.S. Government Printing Office, 1963).

From the preceding discussion, the latter path is undesired except for $X_2 = F_2$, in which case the forward displacement is negligible even at 2000°K. Assigning f to the probability of the path given by eq. (13) and $1-f$ to eq. (12),



The temperature range in which the decomposition of CX_4 is high, and the value of f low, is applicable to RAP crystal growth of the corresponding metal halide.

Two sources of interest to RAP crystal growth with CX_4 are CBr_4 and CCl_4 . We report below the results of studies on the steady-state pyrolysis of these sources and their application to RAP crystal growth of KBr , KCl , and $NaCl$.

Experimental

Figure 1 shows the schematic of the pyrolysis apparatus. The pyrolysis chamber (quartz) is capable of a constant linear flow, i.e., the cross-sectional area of the central tube equals the annular area. At a flow of $1 \text{ cm}^3/\text{sec}$ (carrier gas + RAP agent), the residence time is $\sim 200 \text{ sec}$. A similar design was adopted for the solid source CBr_4 where, for the same flow, the residence time is 20 seconds. The chamber heater was driven with a thermocouple controller ($\pm 5^\circ\text{C}$).

All fittings, stopcocks, and connecting tubings were made of Teflon. The source containers were Pyrex. The CCl_4 bubbler was coarse grade frit. Helium ($>99.99\%$ pure) was the carrier. A 3- and 2-way stopcock arrangement was provided for helium to bypass the source. Pyrex wool and a long vertical section of the tubing leading to the chamber were employed to trap

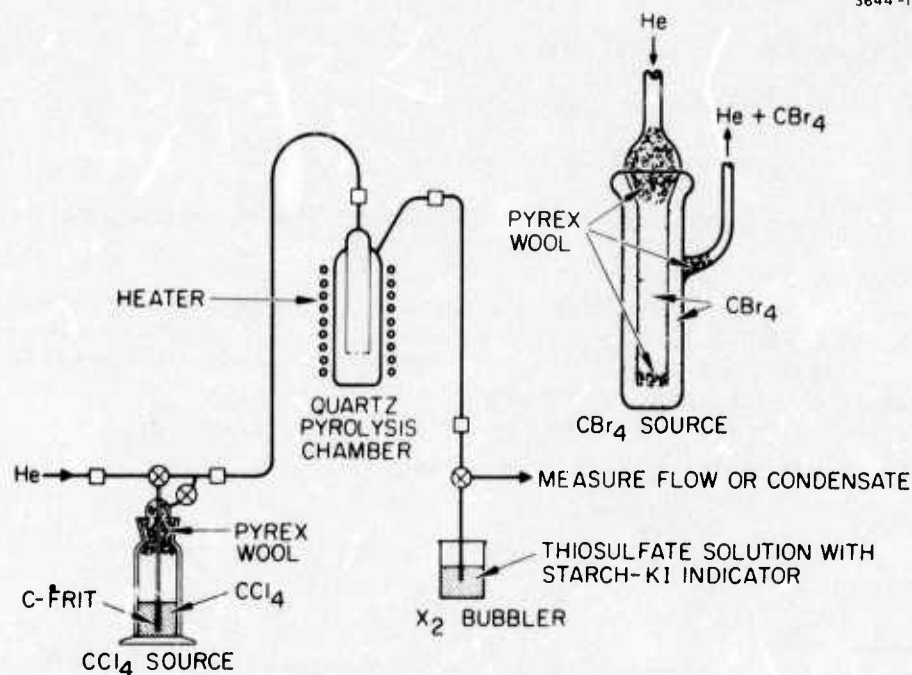


Figure A-1

Schematic of pyrolysis apparatus

entrainment by helium. A flowmeter (upstream, not shown) was used to monitor flow settings but the actual flow was measured at the exit end of the apparatus by water displacement. At the exit, unpyrolyzed CCl_4 was measured by condensation; Br_2 and Cl_2 in the exit gas were chronometrically titrated with a known volume of 0.0201N $\text{Na}_2\text{S}_2\text{O}_3$ using starch-KI indicator. The exit tubing was provided with a heating coil to prevent clogging by the deposit of C_2X_6 .

The source temperature was held at 24°C . At each setting of the pyrolysis temperature, the steady-state flow was determined from five samplings. Five to six titrations followed, spaced at regular time intervals, to determine the steady-state concentration of X_2 in the effluent. The amount of $\text{Na}_2\text{S}_2\text{O}_3$ per titration corresponded to a gas sampling of a volume less than or equal to the volume of the pyrolysis chamber. After the last titration, the flow was again measured.

The RAP crystal growth of KBr and KCl (and NaCl) were carried out in a vertical Bridgman apparatus, using quartz crucibles of 3 to 10 cm i.d. Helium, the carrier gas for the RAP agent (CBr_4 and CCl_4), flowed at $\sim 0.5 \text{ cm}^3/\text{sec}$. The flow arrangement was similar to that used in pyrolysis, with a growth apparatus replacing the pyrolysis chamber. At the exit end, check out titrations were also made but most of the time the exit gas was scrubbed of its X_2 and CX_4 contents with NaOH solution. The melt was soaked for ~ 100 hr and crystal growth was carried out at a lowering rate of 1.5 to 3 mm/hr.

Results and Discussion

Data being unavailable, the saturation pressure of $\text{CBr}_4(\text{s})$ was determined using the CBr_4 -source apparatus (cf. Fig. 1). Helium was the carrier. At a given temperature setting of the source and flow of helium, or residence (saturation) time, the partial pressure of CBr_4 was calculated from the weight loss incurred through a given time interval. Pyrex wool plugs were employed to strip out mechanical entrainment in helium. At constant temperature, the partial pressure increased with decreasing flow, reaching a constant value, the saturation pressure, at a flow $\leq 1 \text{ cm}^3/\text{sec}$, or a residence time ≥ 20 sec. The results are shown in Table 2. The variation of saturation (sublimation) pressure with temperature (cf. Fig. 2) corresponds to an enthalpy change of 14.0 kcal/mole.

TABLE 2
Partial Pressure of $\text{CBr}_4(\text{s})$ Versus Helium Flow

Temperature, $^\circ\text{C}$	Saturation Time, s	Total Flow Time, h	Partial Pressure, mm	Saturation Pressure, mm
0.0	20	18.0	0.0697	0.070 ± 0.000
	35	17.8	0.0702	
23.0	32	16.3	0.462	0.473 ± 0.013
	41	22.5	0.494	
	120	67.0	0.464	
50.0	49	2.5	3.75	3.79 ± 0.04
	72	4.0	3.82	

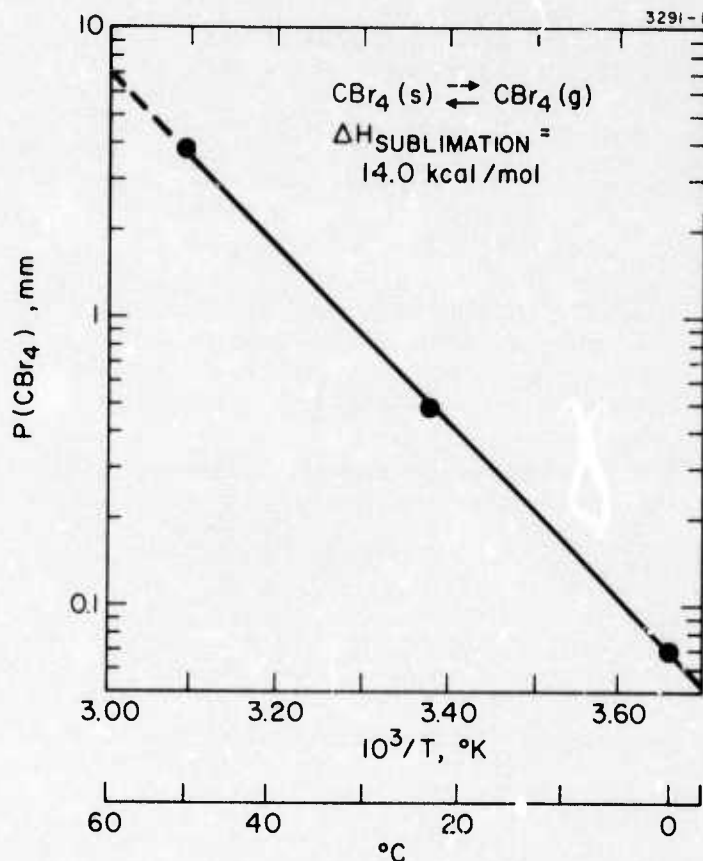


Figure A-2
Sublimation pressure of CBr_4 versus temperature

Pyrolysis measurements were carried out with helium as the carrier at various temperatures (t_p °C). The source temperature was 24°C, which corresponds to a saturation concentration of $c = 2.55 \times 10^{-8}$ mole/cm³ for CBr_4 and $c = 5.40 \times 10^{-6}$ mole/cm³ for CCl_4 . At the exit, the steady-state concentration, $[\text{X}_2]_{\text{SS}}$ in mole/cm³, is

$$[\text{X}_2]_{\text{SS}} = \frac{(\text{moles X}_2)}{vt}, \quad (15)$$

where v is the flow in cm³/sec, t is the time required to attain end-point with a given amount of $\text{Na}_2\text{S}_2\text{O}_3$, and (moles X_2) = (moles $\text{Na}_2\text{S}_2\text{O}_3$)/2. From eq. (14), f can be calculated from

$$[\text{X}_2]_{\text{SS}} = \frac{(3f + 1)c \gamma}{2}, \quad (16)$$

where γ is the fraction of CX_4 unpyrolyzed; $1 - \gamma$ is determined at the exit.

Table 3 gives the results obtained. From the value of f , it is appreciated that RAP crystal growth with CBr_4 is applicable at working temperatures $< 600^\circ\text{C}$. It is not applicable to KBr growth from the melt because at the melting point (730°C) pyrolysis is dominated by eq. (13). However, RAP crystal growth with CCl_4 is applicable up to 900°C and is, therefore, useful to the congruent growth of metal chlorides in general. At the melting point of KCl (776°C), the reaction path shown in eq. (12), i.e., involving the formation of X , is four times favored over that of eq. (13).

As expected, attempts to grow KBr in a quartz crucible by the vertical Bridgman method, have failed with CBr_4 as the RAP source. The melt persisted in wetting the crucible, an indication of partial hydrolysis.* Consequently, although one succeeded in growing a single-crystal ingot, the crystal and/or crucible cracked during cooldown.

* This behavior provides a useful indicator on the reduction of OH^- (or O^{2-}) content in the melt. In the case of fluorides, carbon or platinum crucible serves the same purpose. At very low concentrations of OH^- in RF_3 ($R =$ a rare earth), nonwetting of platinum persists from the liquid (melt) to the solid (crystal).

TABLE 3
Steady State Pyrolysis, CBr_4 Versus CCl_4 (He Flow $< 1 \text{ cm}^3/\text{s}$)

t_p °C	$\text{CBr}_4: 2.55 \times 10^{-8} \text{ mole/cm}^3$			$\text{CCl}_4: 5.40 \times 10^{-6} \text{ mole/cm}^3$		
	γ	f	mole Br_2/cm^3	γ	f	mole Cl_2/cm^3
400	0.17	0.0	0.22×10^{-8}	---	---	---
500	≤ 1.0	≥ 0.11	1.7×10^{-8}	< 0.00	0.0	1.9×10^{-8}
600	1.0	0.48	3.1×10^{-8}	~ 0.20	~ 0.17	0.82×10^{-6}
700	1.0	0.92	4.8×10^{-8}	0.85	0.22	3.8×10^{-6}
800	1.0	1.0	5.2×10^{-8}	< 0.9	> 0.22	4.0×10^{-6}
900	1.0	1.0	5.5×10^{-8}	~ 0.9	~ 0.20	3.9×10^{-6}

The situation was different in the case of KCl and NaCl, grown by the vertical Bridgman method in quartz crucibles with CCl_4 as the RAP source. The single-crystal ingot slipped out easily and the crucibles were reusable over and over. This feature was reproduced in the growth of 3 to 10 cm diameter ingots. Figure 3 is an example of such an ingot (KCl).

A comparison of the steady state effluent, KCl RAP growth versus pyrolysis of CCl_4 , was made. Growth at 800°C , with $v = 0.5 \text{ cm}^3/\text{sec}$, gave 15 millimoles Cl_2 per hour. Pyrolysis at 800°C , with $v = 0.8 \text{ cm}^3/\text{sec}$, gave 12 millimoles Cl_2 per hour.

Noteworthy improvements over previously available materials have resulted in the performance parameters of these anion-ultrapure materials. The measured optical absorption of RAP KCl in a $10.6 \mu\text{m}$ CO_2 laser calorimeter yields an absorption coefficient of 0.00013 cm^{-1} , which value is

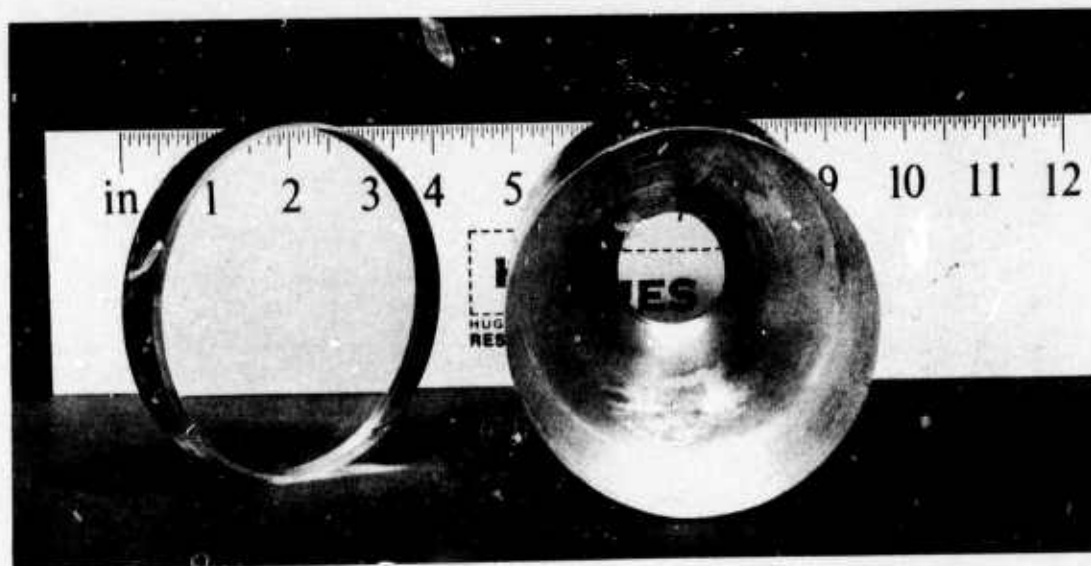


Figure A-3

A 10-cm diameter single-crystal KCl grown by RAP-Bridgman with CCl_4 in He at a flow of $\sim 0.5 \text{ cm}^3/\text{s}$

more than an order of magnitude lower than that of earlier vintage materials (7). Also, with a 0.6 μ s pulse, the CO₂ laser damage threshold of RAP KCl crystal is $>7.8 \times 10^9$ W/cm², which is many orders of magnitude larger than the value reported earlier.* The fracture strength, as measured by 4-point bending (Instron) exceeds 4000 psi, which value is also about one order of magnitude larger.

We are grateful to R. R. Turk of Hughes Research Laboratories for the measurement of fracture strength.

References

1. C.J. Duthler, J. Appl. Phys. 45, 2668 (1974).
2. D. Otterson, J. Chem. Phys. 33, 227 (1960).
3. R.C. Pastor and M. Robinson, Mat. Res. Bull. 9, 569 (1974).
4. D.C. Stockbarger, J. Opt. Soc. Am. 39, 731 (1949).
5. A.H. Sehon and M. Szwarc, Proc. Roy. Soc. A209, 110 (1951).
6. V.I. Vedeneyev, L.V. Gurvich, V.N. Kondrat'yev, V.A. Medvedev and Ye. L. Frankevich, Bond Energies, Ionization Potentials and Electron Affinities. St. Martin's Press, New York, N.Y. (1966).
7. F. Horrigan, C. Klein, R. Rudko, and D. Wilson, Microwaves 8, 68 (1969).

* Laser calorimetry and damage measurements by S.D. Allen of Hughes Research Laboratories (private communication).

APPENDIX B

CRYSTAL GROWTH OF KBr IN A REACTIVE ATMOSPHERE*

R. C. Pastor, A. C. Pastor, and M. A. Aaronson
Hughes Research Laboratories
Malibu, California 90265

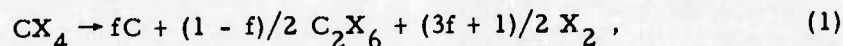
(Received February 6, 1975; Communicated by E. A. Huggins)

ABSTRACT

Reactive atmosphere processing (RAP) with bromomethane derivatives is employed in the crystal growth of KBr (mp = 730°C). Derivatives with higher C-Br bond dissociation energy are found to be applicable.

Introduction

The pyrolysis of carbon tetrahalide, CX_4 , in an inert gas (e. g., He) occurs with two competing reactions,



where $f = 1$ is the undesired path, while $f = 0$ is the desired path where the nascent halogen is an intermediate (1). The objective of the application of reactive atmosphere processing (RAP) to crystal growth is to attain a low value of f in the pyrolytic breakdown of the RAP agent in a temperature range which includes the melting point of the metal halide in question.

Although CBr_4 may prove to be applicable to RAP growth at temperatures well below 600°C, it is inadequate for the growth of KBr (mp = 730°C) because $f = 1$ at temperatures $\geq 700^\circ C$ (1). In the case of $CHBr_3$, it is similarly inadequate for the growth of KBr.

The case of $f = 0$ in eq. (1) may be rewritten to show explicitly the formation of the nascent form of the halogen,



The decay constant, k , of eq. (2) is found to be represented by

$$k = \nu \exp(-D/RT), \quad (3)$$

*This work was supported in part by ARPA Order No. 2612, Contract F33615-74-C-5115, and monitored by the Air Force Materials Laboratory, Wright-Patterson Air Force Base (Ohio).

where ν and D are the C-X bond frequency and dissociation energy, respectively (2). For C-Br, $\nu = 1.75 \times 10^{13} \text{ sec}^{-1}$ (Ref. 3). For crystal growth, the value of k must be constrained to $0 < k < 1$ at the melting point of the metal halide in question. At $k = 0$ no nascent halogen is formed; but at $k \geq 1$, the gas entering the growth apparatus is readily pyrolyzed before reaching the melt and the nascent form is readily lost,



We have shown previously that the molecular halogen form, except in the case of $X_2 = F_2$, is an inadequate RAP agent for the growth of alkali metal halides (1).

At the melting point of KBr, $T = 1003^\circ\text{K}$; for $k < 1$ in eq. (3), it follows that C-Br must have $D > RT \ln v$ or $D > 61 \text{ kcal}$. This constraint provides the basis for explaining the inadequacy of CBr_4 and CHBr_3 to RAP growth of KBr because the values of D are 49 and 56 kcal, respectively (4).

Consequently, other derivatives, $\text{CX}_{4-n}\text{Y}_n$ where $n = 1, 2, \text{ or } 3$, were considered. With Y being an atomic substituent more strongly covalently bonded than X (i. e., H or another halogen), the two parameters, Y and n , provide a graded increase in the dissociation energy of C-X. Thus, in the case of $X = \text{Br}$, the D values for C-Br are (Ref. 4): CBr_4 , 49; CHBr_3 , 56; CH_2Br_2 , 63; CH_3Br , 67; and CF_3Br , 65 (unit: kcal).

An increase in the value of D will shift the onset of pyrolysis to higher temperatures. The choice of Y is such that $D_{\text{C-Y}} > D_{\text{C-X}}$; i. e., thermal dissociation of the C-Y bond should be much less probable than C-X. However, if compounds such as YX ($Y = \text{H}$ and interhalogen radicals) are formed, then the C-Y bond may be ruptured by YX splitting off in the collision of the parent molecule with nascent X or another parent molecule. A good part of the energy required for the C-Y bond rupture is now provided by the energy derived from the formation of the Y-X bond. If YX is not easily dissociated (as in $Y = \text{H}$), the chain-propagation step acts merely as a sink for nascent X (1). If YX is easily dissociated (as in $Y = \text{another halogen}$), the formation of mixed halides in the melt presents a complication.

Experimental

A description of the pyrolysis apparatus and procedure were given previously (1). In the case of the RAP agents, CH_2Br_2 (J. T. Baker Co.) and CF_3Br (Matheson Gas Products), the pyrolysis chamber was laid horizontally to accommodate silica boats loaded with KBr powder, reagent grade (Matheson Coleman and Bell). The pyrolysis residence time was $\sim 200 \text{ sec}$ at a flow of $1 \text{ cm}^3/\text{sec}$. After a run, nonwetting or wetting of the crucible by the melt was deduced by an examination of the polycrystalline cast.

At the exit, the steady-state concentration of Br_2 was measured by the time required to attain endpoint with a given volume of $0.0201 \text{ N Na}_2\text{S}_2\text{O}_3$, using starch-KI solution as the indicator (1). The steady-state concentration of HBr was measured indirectly. Known amounts of N_2H_4 were present in the solution which readily converted Br_2 to HBr. Total HBr was measured by the time required to attain endpoint with a given volume of a freshly made up 0.0603 N NaHCO_3 , using bromocresol green as the indicator. Titration blanks were run to allow for a correction to

unreacted N_2H_4 .

The RAP crystal growth of KBr was carried out in a vertical Bridgman apparatus, using vitreous silica crucibles of 1.7 to 3.2 cm i. d. The flow arrangement was similar to that employed in pyrolysis with the growth apparatus replacing the pyrolysis chamber. The exit gas was scrubbed of its Br_2 and HBr contents with NaOH solution. The melt was soaked for ~ 65 hours and crystal growth was carried out at a lowering rate of ~ 2 mm/hour with CH_2Br_2/He , while in the case of CF_3Br/He , the soak was ~ 3 hours and the lowering rate was ~ 5 mm/hour.

The single-crystal ingots of KBr were cut into cylinders with a string saw. An optical finish at the ends was obtained by polishing with Linde A in methanol. The infrared transmission in the wavelength range of 2.5 to 25 μm was measured with an infrared spectrophotometer (Beckman IR 12).

Results and Discussion

When the f value of eq. (1) is not close to zero, we have shown in the case of CCl_4 , that a reactive carrier gas such as CO_2 can be used to eliminate the carbon deposit which accumulates during crystal growth, and the product, CO, is able to tie up free Cl_2 as $COCl_2$ (Ref. 5). In the case of CBr_4 , where $f \approx 1$ at temperatures $> 600^\circ C$, the gettering reaction of CO_2 on C is not able to keep up with the $f = 1$ path of eq. (1). A thick carbon deposit forms in the pyrolysis of CBr_4/He and CBr_4/CO_2 . More efficient thermalization by CO_2 is seen in the heavier deposit of C upstream, indicating that pyrolysis occurs at a lower temperature region and at a low fraction of the total residence time. At the low-temperature region, the reaction of CO_2 on C, to form CO, is too slow. As seen in Table I, there is also no evidence of a decrease in halogen concentration with increase in temperature when the carrier gas is changed from He to CO_2 , i. e., negligible formation of $COBr_2$.

The results of pyrolysis of CH_2Br_2/He is collected in Table II. As seen in the second column, the total flow was 0.43 ± 0.01 cm³/sec, and this is equivalent to a residence time of ~ 7 min in the pyrolysis chamber. The furnace was held at $200^\circ C$ for 19 hours to dry the KBr. The third column gives the CH_2Br_2 content of the carrier gas (He) at a $25^\circ C$ saturation.

The fourth and fifth columns show that Br_2 and HBr formations start as low as $200^\circ C$. While Br_2 formation increases up to $500^\circ C$ and drops with further increase in temperature; HBr formation increases monotonically with temperature. At $500^\circ C$, the HBr concentration is one order of magnitude larger than that of free Br_2 , and at $900^\circ C$, the concentration ratio is $\sim 10^3$. These results indicate that gas-phase formation of HBr at low temperatures from CH_2Br_2 , unimolecularly or bimolecularly, occur. The drop in the concentration of free Br_2 at the higher temperatures suggests a second mechanism for the formation of HBr, i. e., reaction of nascent Br or molecular Br_2 with CH_2Br_2 . Although the C-H bond in CH_2Br_2 has a bond energy $D = 99$ kcal (Ref. 4), scission requires an investment of only 11 kcal because $D = 88$ kcal for HBr (4). This is for the case of nascent Br. For molecular Br_2 , the investment is 57 kcal, which value is still less than the C-Br value for CH_2Br_2 ($D = 63$ kcal).

From the preceding analysis of the pyrolysis of CH_2Br_2/He , one would expect that only a very small fraction of HBr results from the attack of

nascent bromine on the OH^- impurity in the RAP growth of KBr. The gas-phase formation of HBr favors a lower RAP-index (1) but not at the expense of the H_2O species being converted to HBr at a 1:2 stoichiometry. Repeated crystal growth runs indicated that CH_2Br_2 may still be a borderline case RAP agent for the growth of KBr. Sections of the ingot adhered to the crucible (vitreous silica).

TABLE I

Pyrolysis of CBr_4/He and CBr_4/CO_2

$^{\circ}\text{C}$	(Mole Br_2/cm^3) $\times 10^8$ ^a	
	CBr_4/He	CBr_4/CO_2
400	0.22	—
500	1.7	—
600	3.1 ± 0.1	3.2 ± 0.1
700	4.8 ± 0.2	4.7 ± 0.1
800	5.2 ± 0.2	5.2 ± 0.2
900	5.5 ± 0.4	5.4 ± 0.3

^aSaturation of carrier gas between 24 to 25 $^{\circ}\text{C}$ corresponds to (mole Br_2/cm^3) $\times 10^8 = 5.5 \pm 0.4$ at 100% pyrolysis.

TABLE II

Pyrolysis of $\text{CH}_2\text{Br}_2/\text{He}$

$^{\circ}\text{C}$	Input		Output		Pyrolysis, ^d %
	Total Flow, cm^3/sec	A ^a	B ^b	C ^c	
200	0.44	1.04	< 1.06	< 1.8	< 0.18
400	0.44	1.03	3.79	43	4.2
500	0.43	1.03	11.9	163	16
600	0.43	1.01	7.09	189	18.7
700	0.43	1.01	1.95	192	19.0
800	0.43	1.01	< 1.0	217	21
900	0.42	1.01	< 0.50	244	24

^aA = (mole $\text{CH}_2\text{Br}_2/\text{sec}$) $\times 10^6$, equals the theoretical output of (mole Br_2/sec) $\times 10^6$ for 100% pyrolysis.
^bB = (mole Br_2/sec) $\times 10^9$ by thiosulfate titration.
^cC = (total mole Br_2/sec) $\times 10^9$ from Br_2 and $\text{HBr}/2$.
^dPyrolysis % = $C/(10A)$.

The above results suggested the use of CF_3Br instead of CH_3Br . A 10 mole% mixture in He was obtained (Matheson Gas Products). Molecular weight determination with a 5-liter bulb (Regnault method) showed the composition to be 11.4 ± 0.2 mole%. The pyrolysis furnace, with $\text{CF}_3\text{Br}/\text{He}$ flowing at $\sim 0.3 \text{ cm}^3/\text{sec}$, was held at 200 $^{\circ}\text{C}$ for 15 hours to dry the KBr. Table III gives a summary of the results obtained in the pyrolysis of $\text{CF}_3\text{Br}/\text{He}$.

Unlike the case of $\text{CH}_2\text{Br}_2/\text{He}$ (cf. Table II), Table III shows that Br_2 formation increases monotonically with temperature in the pyrolysis of $\text{CF}_3\text{Br}/\text{He}$. Although the bromine-atom content of the gas entering is about a factor of two larger in $\text{CH}_2\text{Br}_2/\text{He}$ (compare the A values), note that at 800 $^{\circ}\text{C}$ the Br_2 output is about three orders of magnitude smaller than that of $\text{CF}_3\text{Br}/\text{He}$. No visible deposit of C in the melt resulted, i. e., low f value in eq. (1). The frozen KBr showed that the melt assumed a nonwetting meniscus. Naturally, the polycrystalline ingot was easily removed from the quartz boat. Figure 1 shows the polished pieces of KBr fabricated from the ingots grown under $\text{CH}_2\text{Br}_2/\text{He}$ and $\text{CF}_3\text{Br}/\text{He}$.

The infrared transparency of these specimens was examined with the Beckman IR 12. The KBr grown in $\text{CH}_2\text{Br}_2/\text{He}$, diameter = 3.0 cm and length = 1.4 cm, showed a flat transmission from 2.5 to 18 μm and the knee of the curve was at 20 μm , in agreement with the behavior reported in the literature (6). The KBr grown in $\text{CF}_3\text{Br}/\text{He}$, diameter = 1.6 cm and

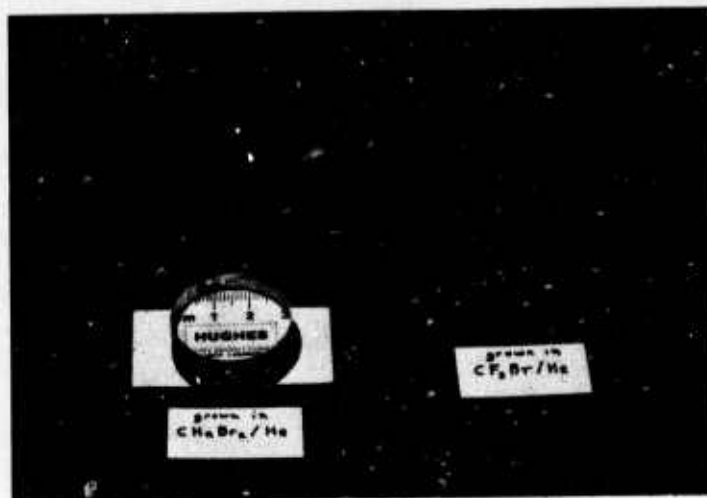


Figure B-1

RAP grown single crystal KBr.

length = 4.7 cm, showed, in addition, two small sharp absorption bands at 12 and 13 μm corresponding to an absorption coefficient of $\sim 0.008 \text{ cm}^{-1}$. After the specimen was repolished, the 12- μm absorption coefficient was $\sim 0.004 \text{ cm}^{-1}$ while the 13- μm was $\sim 0.010 \text{ cm}^{-1}$. Another specimen, with the same diameter but a length of 10 cm, showed no 12- μm absorption and the 13- μm absorption coefficient was $\sim 0.007 \text{ cm}^{-1}$. Hence, the 12- μm absorption came from the surface. The 13- μm absorption came from the bulk and could be due to an anion impurity, e. g., fluoride from CF_3Br pyrolysis. Further evaluation is in progress and will be reported in the near future.

TABLE III

Pyrolysis of $\text{CF}_3\text{Br}/\text{He}$

$^{\circ}\text{C}$	Input		Output	Pyrolysis, ^c %
	Total Flow, cm^3/sec	A ^a	B ^b	
600	0.26	1.23	20.4	3.3
700	0.27	1.25	95.3	15.2
800	0.29	1.37	340	49.6

^aA = (mole $\text{CF}_3\text{Br}/\text{sec}$) $\times 10^6$ and half this value is the theoretical (mole Br_2/sec) $\times 10^6$ for 100% pyrolysis.

^bB = (mole Br_2/sec) $\times 10^9$ by thiosulfate titration.

^cPyrolysis % = 0.2 B/A.

References

1. R. C. Pastor and A. C. Pastor, *Mat. Res. Bull.* 10, No. 2 (1975).
2. A.H. Sehon and M. Szwarc, *Proc. Roy. Soc.* A209, 110 (1951).
3. L.J. Beilamy, *The Infra-Red Spectra of Complex Molecules*. John Wiley and Sons, Inc., New York (1956).
4. V.I. Vedeneyev, L.V. Gurvich, V.N. Kondrat'yev, V.A. Medvedev, and Ye.L. Frankevich, *Bond Energies, Ionization Potentials, and Electron Affinities*. St. Martin's Press Inc., New York (1966).
5. R. C. Pastor and A. C. Pastor, submitted to *Mat. Res. Bull.*
6. See page 36 of *Harshaw Optical Crystals*, Copyright 1967, from the Harshaw Chemical Co. (Ohio). See also Bulletin 50, *Optical Crystals*, 1969, from Optovac Inc. (Mass.).

APPENDIX C

CRYSTAL GROWTH OF KCl IN A REACTIVE ATMOSPHERE*

R.C. Pastor and A.C. Pastor
Hughes Research Laboratories
Malibu, California 90265

(Received February 14, 1975; Communicated by R. A. Huggins)

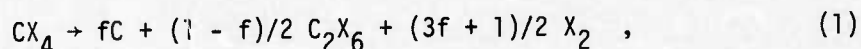
ABSTRACT

Reactive atmosphere processing (RAP) with CCl_4 is employed in the crystal growth of KCl (mp = 776°C). Two carrier gases, He and CO_2 , are compared. A carbon deposit accumulates in the growth of KCl in CCl_4/He , a drawback which is eliminated in crystal growth under CCl_4/CO_2 .

Introduction

In a previous publication, certain concepts of reactive atmosphere processing (RAP), as applied to crystal growth, were discussed (1). It was pointed out that the pseudohalide impurity, OH^- , poses a special problem because H_2O , its source, is always present in all steps of processing, including crystal growth. To achieve a low ratio of OH^- to X^- (halide ion) in the condensed phase, the chosen reaction must be capable of constraining the gas phase to a very low value of the RAP-index, $P(\text{H}_2\text{O})/P(\text{HX})$.

For crystal growth of the corresponding metal halide, CX_4 was chosen in the study as the RAP agent because of its capability to provide the nascent form of the halogen (2). Unfortunately, in CX_4 the pyrolysis in an inert carrier (He) occurs with two competing reactions,



where $f = 1$ is the undesired path, while $f = 0$ is the desired path where the nascent halogen is an intermediate (1).

The objective in RAP crystal growth is to attain a low value of f in the pyrolytic breakdown of the RAP agent over a temperature range which includes the melting point of the metal halide. Thus, CBr_4 proved to be an inadequate RAP agent for the growth of KBr (mp = 730°C) because $f = 1$ at temperatures $\geq 700^\circ\text{C}$, while CCl_4 was applicable to the growth of KCl (mp = 776°C) because the $f = 0$ path was four times more probable than the $f = 1$ path from 700 to 900°C (1).

*This work was supported in part by ARPA Order No. 2612, Contract F33615-74-C-5115, and monitored by the Air Force Materials Laboratory, Wright-Patterson Air Force Base, Ohio.

The above studies were carried out with an inert carrier (He). A drawback in the growth of KCl under CCl_4/He arises because the value of f is not close to zero. For long processing times, the generation and accumulation of C and Cl_2 lead to various problems. The deposited C may be a contributing factor to significant deviations of the ingot from monocrystallinity and, not infrequently, greatly reduces the utilizable fraction. The excessive buildup in Cl_2 provides the limiting factor to the lifetime of the growth apparatus. With the object of overcoming these drawbacks, a reactive carrier gas was studied. We report here the results of such a study using CO_2 as the carrier gas for CCl_4 .

Experimental

A description of the pyrolysis apparatus and procedure was given previously (1). The temperature of the source (CCl_4) was held at 24°C , which corresponds to a saturation concentration of 5.40×10^{-6} mole CCl_4/cm^3 in the gas phase.* The total flow of carrier gas and CCl_4 was maintained at ~ 0.8 cm^3/sec or a residence time, τ , in the pyrolysis chamber of ~ 4 min. The CCl_4 liquid is reagent grade (J.T. Baker Chemical Company). The purity of He was $>99.99\%$ (Airco) and CO_2 was $>99.9\%$ (Matheson Gas Products).

At the exit, the steady-state concentration of Cl_2 was measured by the time required to attain endpoint with a given volume of $0.0201 \text{ N Na}_2\text{S}_2\text{O}_3$, using starch-KI solution as the indicator (1). The total flow was measured by water displacement.

The RAP crystal growth of KCl was carried out in a vertical Bridgman apparatus, using vitreous silica crucibles of 3 cm i.d. The carrier gas (He or CO_2) for CCl_4 flowed at ~ 0.5 cm^3/sec . The flow arrangement was similar to that used in pyrolysis, with the growth apparatus replacing the pyrolysis chamber. At the exit, titrations for Cl_2 have been made which check out with the results of pyrolysis (1). The exit gas was scrubbed of its Cl_2 and CCl_4 contents with NaOH solution. The melt was soaked for ~ 65 hour and crystal growth was carried out at a lowering rate of ~ 2 mm/hour.

The single-crystal ingots were cut into 10-cm length cylinders with a string saw. An optical finish at the ends was obtained by polishing with Linde A in methanol. The infrared transmission in the wavelength range of 2.5 to 20 μm was measured with an infrared spectrophotometer (Beckman IR 12).

Results and Discussion

A comparison of the steady-state concentration of Cl_2 in the effluent in the pyrolysis of CCl_4/He and CCl_4/CO_2 , at approximately equal residence times, τ , in the pyrolysis chamber, is given in Table I.

It is seen that at 500°C , the rate of halogen formation is $\sim 200\%$ higher in the CO_2 carrier. This feature may be explained by the difference in molecular mass and heat capacity of the carriers, CO_2 being the more efficient thermalizing agent. The difference in the rate decreases with an increase in the pyrolysis temperature; the crossover is at 700°C . From 700 to 800°C , the rate of halogen formation increases with He carrier gas but decreases with CO_2 . The latter behavior is due to a significant reactivity

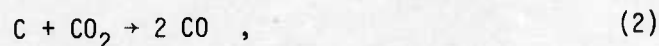
* Complete pyrolysis by $f = 0$ path in eq. (1) yields 1.08×10^{-5} mole Cl_2/cm^3 and by $f = 1$ path, 2.70×10^{-6} mole Cl_2/cm^3 .

TABLE I
Pyrolysis of CCl_4/He and CCl_4/CO_2

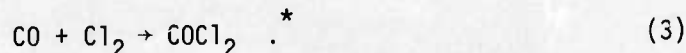
$^{\circ}\text{C}$	CCl_4/He		CCl_4/CO_2	
	τ , min	$A \times 10^{8a}$	τ , min	$A \times 10^{8a}$
500	3.9	0.94	3.8	2.8
600	3.7	41.2	3.9	49.0
700	3.8	191	4.1	191
800	3.7	201	4.1	181

^aA = mole Cl_2/cm^3 in the effluent.

of CO_2 to the carbon deposit resulting from the $f = 1$ branch of eq. (1),



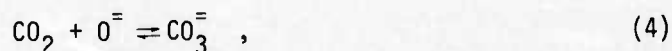
and the resulting CO tying up the free chlorine (3),



For a 20-hour pyrolysis at 800°C , a light carbon deposit formed in CCl_4/He but none in CCl_4/CO_2 . This feature was reproduced in crystal growth as seen in Fig. 1. Note in the case of the KCl ingot grown from CCl_4/He that the last one-eighth fraction cannot be utilized as it is densely packed with bubbles.

Window specimens, 10 cm in length, were fabricated from the ingots shown in Fig. 1 for infrared transmission measurement in the Beckman IR 12. The transmission curve was flat at ~94% transmission from 2.5 to 12.5 μm with the knee of the curve at 14.5 μm for both specimens. In the ten μm range, the deviations are $\leq 0.5\%$ which result indicates that the absorption coefficient at 10.6 μm (CO_2 laser calorimetry) would differ by $\leq 0.0005 \text{ cm}^{-1}$ between the two specimens.

The results of infrared transmission measurements are significant to the objective of RAP growth, viz., removal of anion impurities. With CO_2 as the carrier, the presence of O^- and OH^- impurities in the melt would have led to the formation of CO_3^- and HCO_3^- impurities, respectively:



and

* It is not unlikely that the bimolecular reaction, $\text{CO}_2 + \text{CCl}_4 \rightarrow 2 \text{COCl}_2$, is occurring in the gas phase; hence, two sources for COCl_2 . The latter hydrolyzes easily and is removed from the exit gas by the scrubber, $\text{COCl}_2 + 2 \text{NaOH} \rightarrow 2 \text{NaCl} + \text{H}_2\text{O} + \text{CO}_2$.

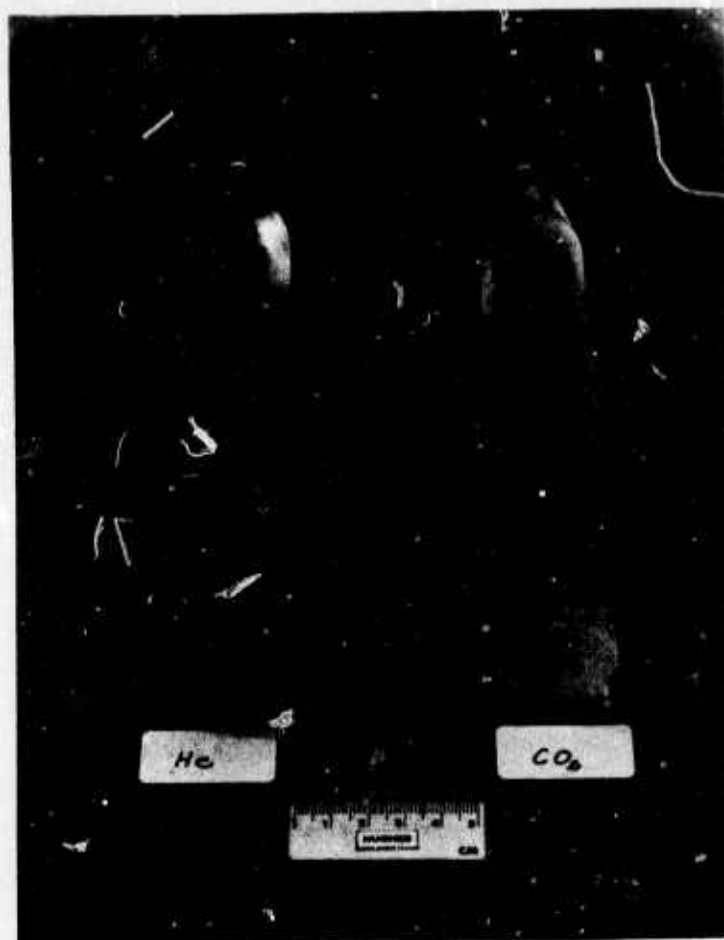


Figure C-1

Bridgman KCl ingots grown under CCl_4/He and CCl_4/CO_2 .



In 10-cm length KCl, an impurity level of 100 ppm $\text{CO}_3^{=}$ would have shown absorption bands from 6.6 to 14.7 μm , while 0.1 ppm HCO_3^- would have given absorption bands from 3.0 to 15.9 μm (4).

From eqs. (4) and (5), one can show that the $\text{HCO}_3^-/\text{CO}_3^{=}$ ratio is dependent on the OH^-/O^- ratio which, in turn, is dependent on H_2O . It will be recalled that the latter is governed by the RAP-index. The results obtained indicate that the RAP growth procedure provides a very low value of the RAP-index and also effects an efficient removal of O^- impurity in the condensed phase.

We thank M. Aaronson for the infrared transmission measurements on the KCl crystals.

References

1. R.C. Pastor and A.C. Pastor, Mat. Res. Bull. 10 No. 2 (1975).
2. A.H. Sehon and M. Szwarc, Proc. Roy. Soc. A209 110 (1951).
3. See p. 403, Mellor's Modern Inorganic Chemistry, edited by G.D. Parkes (Longmans, 1967).
4. C.J. Duthler, J. Appl. Phys. 45 No. 6, 2668 (1974).

APPENDIX D

CRYSTAL GROWTH OF ALKALINE EARTH FLUORIDES
IN A REACTIVE ATMOSPHERE*

R.C. Pastor and K. Arita
Hughes Research Laboratories
Malibu, California 90265

(Received April 4, 1975; Communicated by R. A. Huggins)

ABSTRACT

Crystal growth of MF_2 ($M = Ca, Sr, \text{ or } Ba$) is carried out in a reactive atmosphere consisting of HF and a carrier gas (He). Single-crystal Bridgman ingots, with the axis oriented at $\langle 111 \rangle$, are grown up to 5.2 cm in diameter. The mechanical strength of these specimens is found to be higher than what has been reported.

Introduction

The ubiquity of water is responsible for the almost universal presence of hydroxide ions in halide crystals prepared without special attention to excluding water. For crystals grown from the melt, hydroxide contamination occurs through hydrolysis:



Equation (1) shows that in the presence of water in the gas phase (g), a halide ion (X^-) in the condensed phase (c) is replaced by a hydroxyl ion (OH^-) with the production of the hydrogen halide (HX). From the equilibrium relation, the concentration ratio C , of OH^- to X^- in the solid, is given by:

$$C = K \frac{P(H_2O)}{P(HX)} \quad (2)$$

where K is the equilibrium constant and the P s are partial pressures.

Since the objective is to achieve a low value of C , one must remove the H_2O and provide HX . The use of vacuum or an inert gas is not wholly

*This work was supported in part by Contracts F33615-73-C-5075 and F33615-74-C-5115 (ARPA Order No. 2612) of the Air Force Materials Laboratory, Wright-Patterson Air Force Base (Dayton, Ohio).

effective in achieving a small C because $P(H_2O)$ is never zero, while $P(HX)$ is essentially zero in those circumstances. The reactive atmosphere processing (RAP) technique employed in the crystal growth of alkaline-earth fluorides (cf. below) differs from the preceding methods in that it provides gaseous HF to drive the equilibrium of eq. (1) to the left.

Control of the RAP-index, $P(H_2O)/P(HX)$, to a very low value during crystal growth of chlorides and bromides significantly improved the crystal's mechanical strength, infrared transparency, and resistance to laser damage (1). In the case of fluorides, such control prevented the occurrence of solid-solid transitions (2), increased the melting point (3), led to a different solid-solution behavior (4), and caused melting-congruency behavior in a system reported to undergo a peritectic reaction (5). We report here the extension of these studies to the growth of the alkaline-earth fluorides.

Experimental

The starting materials were MF_2 powders (EM Laboratories) which were rated better than five-nines pure with respect to the cation. In the case of BaF_2 , the powder was also prepared from five-nines pure $BaCO_3$ (J. Matthey), using 49% HF solution and completing the conversion with HF gas (3).

A graphite resistance furnace (Astro Industries) was used to grow the crystals by a vertical Bridgman mode. Vitreous carbon crucible (Beckwith Corporation) was used in the growth of 3-cm diameter ingots by spontaneous nucleation. For 4.3- and 5.2-cm diameter growth, graphite crucibles were fabricated in our shop with the design shown in Fig. 1(a). A seed well was provided for oriented growth at $\langle 111 \rangle$. Loading of the crucible plus MF_2 powder charge in the furnace is followed by leak checking, vacuum pumping, and RAP at a low temperature before melting. The reactive atmosphere consisted of HF (99.9%, H_2O -content = few ppm) diluted to 10 mole % with He flowing at 2 l/min. The melt is soaked for eight hours; then growth proceeds with the crucible lowered at 2.5 mm/hour and rotated at 1 rpm. After completion of crystal growth the temperature is lowered to room temperature over a 13-hour period by a cam on the temperature controller. Figure 1(b) shows the three sizes of MF_2 ingots grown.

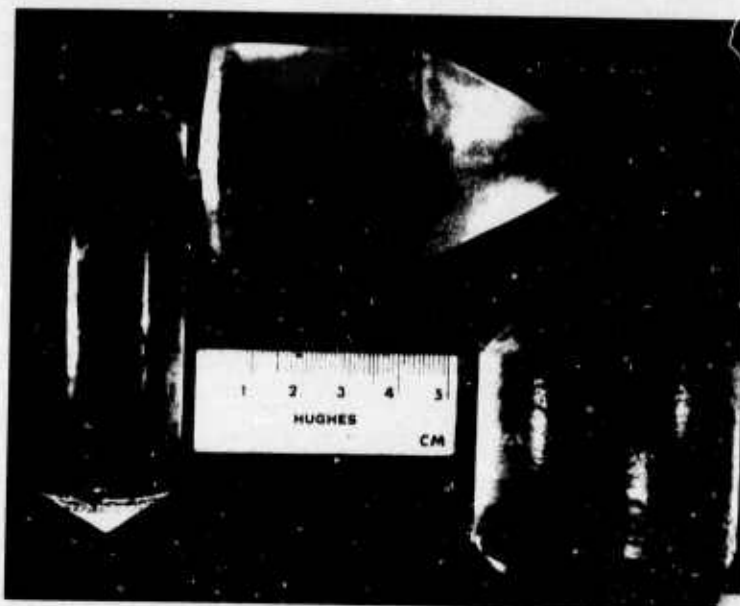
The $\langle 111 \rangle$ orientation of the 4.3- and 5.2-cm diameter ingots were verified by x-ray back reflection (Laue) on the portion of the raw ingot which crystallized last. The microhardness (Knoop) and the mechanical strength (Instron) were determined on unoriented specimens. To determine the infrared transparency from 2.5 to 10 μm (Beckman IR 12), windows were fabricated by cutting with a wet diamond-impregnated wire and given a final polish with an aqueous suspension of Linde A.

Results and Discussion

The results of the emission spectrograph analysis of the MF_2 powders as received from EM Laboratories are collected in Table I. It is seen that the major impurities are other members of the alkaline earths. A comparison of the analysis of the powder and the crystal tail, which corresponds to the initial and final bulk melt compositions respectively, show in the case of CaF_2 that the last section to crystallize is five times richer in magnesium while strontium is constant at 0.04 ± 0.01 wt%. The behavior of Mg^{+2}



(a)



(b)

Figure D-1

Crystal Growth of MF_2

- (a) Design of the graphite crucible for the vertical Bridgman growth of MF_2 single-crystal ingot oriented in the $\langle 111 \rangle$ direction.
 (b) Scale up in the crystal growth of MF_2 : ingot diameter 3.0, 4.3, and 5.2 cm.

TABLE I
 Emission Spectrograph Analysis* of EM Ultrapure MF_2 Powders

	CaF_2	SrF_2	BaF_2
Mg	0.012	0.00013	0.00014
Ca	51.	0.0050	0.0052
Sr	0.052	70.	0.019
Ba	ND < 0.01	ND < 0.01	78.
Fe	ND < 0.002	ND < 0.0005	ND < 0.002
Mn	ND < 0.001	ND < 0.0002	ND < 0.001
Cu	ND < 0.000005	TR < 0.00005	ND < 0.000005
Al	TR. 0.001	0.00054	ND < 0.0007
Si	0.0071	0.021	0.0084

*Reported as weight percent by Pacific Spectrochemical Laboratory, Inc., Los Angeles, California

(partition coefficient <1) implies fine precipitation of MgF_2 in eutectic formation if, indeed, CaF_2 - MgF_2 has no region of solid-solution formation(6). The behavior of Sr^{+2} is in accord with the claim that CaF_2 - SrF_2 forms a continuous solid solution with a shallow minimum (7). The behavior of Ba^{+2} in the crystallization of SrF_2 (or Sr^{+2} in BaF_2 crystallization) is in agreement with the solid-solution behavior reported for BaF_2 - SrF_2 which exhibits a shallow minimum at 19 ± 1 wt% Sr (8). In the crystallization of BaF_2 , both Mg^{+2} and Ca^{+2} show the behavior corresponding to a partition coefficient less than unity. The partition behavior of the 3d ions, chromium to copper, indicates a coefficient less than unity. The concentration of Al^{+3} in the crystal tail is more than an order of magnitude lower than that of the powder, which is to be expected from the much higher volatility of AlF_3 . The concentration of silicon remains stationary and would seem to be due to leaching of the crucible.

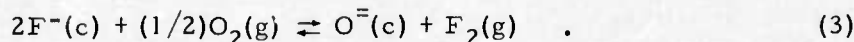
The measured Knoop hardness (unoriented specimens) is: CaF_2 , 160 kg/mm^2 ; SrF_2 , 140 kg/mm^2 ; and BaF_2 , 90 kg/mm^2 . These values are consistently higher than those given for commercial MF_2 : CaF_2 , 120 kg/mm^2 ; SrF_2 , 130 kg/mm^2 ; and BaF_2 , 65 kg/mm^2 (9). Compared to the commercial specimens, RAP grown BaF_2 shows the more dramatic improvement in structural integrity.

The increase in hardness accompanies the closeness in crystal packing. For an F^- ion radius of 1.36 Å, the volume occupied by one Avogadro number is 12.1 cm^3 (fluorite structure). The experimental values are: 12.3 cm^3 for CaF_2 , 14.8 cm^3 for SrF_2 , and 17.9 cm^3 for BaF_2 .

That low-level hydrolysis degrades mechanical performance is indicated by the comparison of LiF , air-grown versus that grown in vacuum (10). The latter method yields a specimen that is less hydrolyzed, but still not completely free of OH^- . The improvements for the less hydrolyzed specimen were as follows: Young's modulus, from 1.02×10^7 to 1.12×10^7 psi; elastic limit, from 1200 to 3900 psi; and modulus of rupture, from 2100 to 5200 psi. The ultimate strength (modulus of rupture) of commercial MF_2 is: CaF_2 , 4500 psi; SrF_2 , 6100 psi; and BaF_2 , 2900 psi (11). Our strength tests on RAP-grown CaF_2 show a modulus of rupture $>12,000$ psi. There being no yield point, these values are limited by surface defects in fabrication.

The long path-length IR spectra of RAP single-crystal CaF_2 , SrF_2 , and BaF_2 are shown in Fig. 2. From 2.5 μm , it is seen that good transparency is exhibited by CaF_2 up to 7 μm and SrF_2 up to 8 μm . In the case of BaF_2 , the apparent transparency up to 9 μm is marred by a few absorption bands. A different absorption spectrum resulted from a 5-cm long BaF_2 crystal prepared from five-nines pure $BaCO_3$. The comparison indicates that the extraneous absorptions are not intrinsic to the material. An additional one-hour RAP soak of the BaF_2 melt at $\sim 250^\circ C$ above its melting point led to the removal of these absorption bands.

We conclude from these observations on RAP growth that the various improvements resulted from a displacement of eq. (1) to the left, to a greater extent than can be realized with the use of an inert gas or vacuum. The oxide ion impurity is not introduced directly by displacement (oxidation),



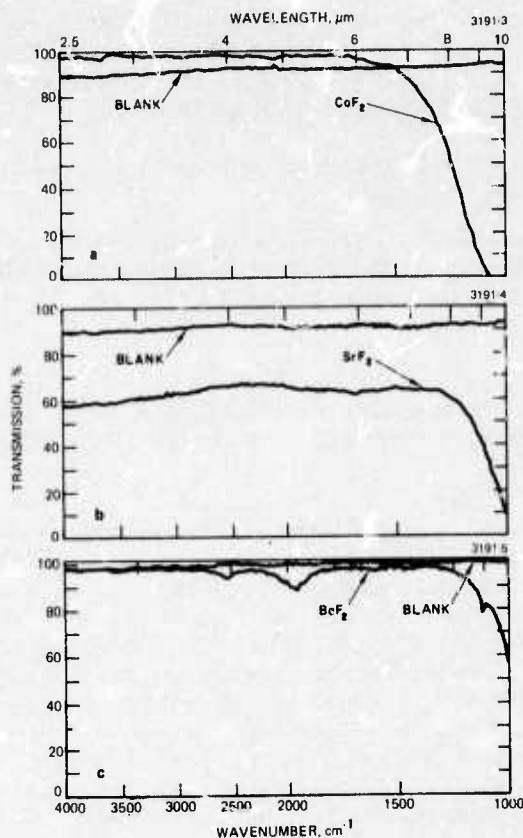


Figure D-2

IR Transmission of RAP Crystals.

- (a) CaF_2 , 3.4-cm thick
- (b) SrF_2 , 5.2-cm thick
- (c) BaF_2 , 5.2-cm thick

Extrapolation of the thermodynamic properties of CaF_2 to its melting point (1700°K) shows that at $P(\text{O}_2) = 0.2$ atm, the equilibrium pressure of fluorine in eq. (3) is ~ 10 -12 atm (12). Thus, for practical purposes, the fluorite lattice cannot be oxidized directly. However, the $\text{O}^=$ impurity can result indirectly,



Equation (4) is dependent on the forward progress of eq. (1) which, in turn, is dependent on the RAP-index. The marked resistance of CaF_2 to dry O_2 and its low resistance to corrosion by traces of H_2O have been demonstrated (13). Sensitivity to the dewpoint of the outgas is seen in the annealing of CaF_2 at 1000°C under a vacuum of 10^{-5} mm Hg. After a two-hour soak, the material was found to be covered on the surface with a 0.5- μm thick white deposit. The degradation of the ultraviolet transmission of MF_2 by heat treatment in vacuum has been reported (14).

Can we expect to improve further on the present RAP approach to the growth of MF_2 ? Three calculations are outlined which favor the affirmative answer. First, there are two reasons which account for HF being the poorest RAP agent among the hydrogen halides (HX) in eq. (1):

1. Unlike HCl, HBr, and HI, the free energy of formation (ΔG) of HF is lower than that of H_2O .
2. With increasing T, $\Delta G(HF)$ decreases while $\Delta G(H_2O)$ increases. The fluorides have the lowest ΔG among the alkaline-earth halides. The consequent high T_{mp} of the fluoride leads to a high temperature RAP.

Second, it has been shown in the case of the best HX RAP agent (HCl) that other RAP agents are capable of providing a much lower RAP-index, e.g., CCl_4 (Ref. 1). With HX(g), the RAP-index is limited by the sources of $H_2O(g)$ present.

The third calculation indicates that the steady-state RAP-index during growth is not determined by the H_2O -content of HF(g) but by the dewpoint of the outgas. The effect is gauged to a first approximation by assuming the steady-state operation to be not far removed from equilibrium, and K of eq. (1) is dependent only on T. The enthalpy change for hydrolysis (in the case of CaF_2) is approximately constant at 25.1 kcal/mole from 1420°K (T_{mp} of HoF_3) to 1700°K (T_{mp} of CaF_2). It follows from the extrapolated thermodynamic properties that $K = 0.055$ at 1700°K and $K = 0.012$ at 1420°K. Infrared absorption at 2.8 μm and 77°K of HoF_3 yields $C = 10^{-5}$ (Ref. 2). Hence, at 1420°K, the effective RAP-index is $\sim 10^{-3}$, which value is three orders of magnitude larger than the H_2O -content of HF(g).

Experiments are in progress which show that much lower values of the RAP-index can be achieved during crystal growth. These results will be reported in the near future.

Acknowledgments

We are grateful for the assistance of the following colleagues in the Laboratory: A.C. Pastor for the crystal growth crucible design, M. Robinson for assistance in crystal growth, K.T. Miller for carrying out Laue x-ray check on crystal orientation, G. Heussner for the fabrication of test specimens (optical and mechanical), R.R. Turk for mechanical testing, and M.A. Aaronson for the measurement of infrared transparency.

References

1. R.C. Pastor and A.C. Pastor, Mat. Res. Bull. 10, 117 (1975).
2. R.C. Pastor and M. Robinson, Mat. Res. Bull. 9, 569 (1974).
3. R.C. Pastor and K. Arita, Mat. Res. Bull. 9, 579 (1974).
4. R.C. Pastor, A.C. Pastor, and K.T. Miller, Mat. Res. Bull. 9, 1247 (1974).
5. R.C. Pastor, M. Robinson, and W. Akutagawa, submitted to Mat. Res. Bull.

6. M. Rolin and M. Clausier, *Rev. Int. Hautes Temp. Refract.* 4, 43 (1967). These authors show a simple binary with the eutectic at 44.4 wt % MgF_2 and 980°C .
V.T. Bereznnaya and G.A. Bukhalova, *Russ. J. Inorg. Chem.* 6, 1091 (1961). The eutectic is characterized as 58% MgF_2 and 948°C .
7. P.F. Weller, J.D. Axe, and G.D. Petit, *J. Electrochem. Soc.* 112, 74 (1965). The minimum is near 50 mole % SrF_2 and 1330°C .
8. Ralph H. Nafziger, *J. Amer. Ceram. Soc.* 54, 467 (1971).
9. See Table 2, "Harshaw Optical Crystals," The Harshaw Chemical Co. (1967).
10. L.S. Combes, S.S. Ballard, and K.A. McCarthy, *J. Opt. Soc.* 41, 215 (1951).
11. F.A. Horrigan and T.F. Deutsch, "Research in Optical Materials and Structures for High Power Lasers," Table III, Raytheon Research Division (Waltham, Mass.), Second Quarterly Report (December 1970), U.S. Army Missile Command (Redstone Arsenal, Alabama), ARPA Order No. 1180.
12. C.E. Wicks and F.E. Block, "Thermodynamic Properties of 65 Elements -- Their Oxides, Halides, Carbides, and Nitrides," Bulletin 605, Bureau of Mines, United States Department of the Interior (U.S. Government Printing Office, Washington, D.C.: 1963).
13. W. Bontinck, *Physica*, 24, 650 (1958).
14. E.G. Chernevskaya, *J. Applied Spectroscopy*, 14, 225 (1971).

APPENDIX E

APPROACH TO EQUILIBRIUM IN THE DISSOCIATION OF X_2

The dissociation of X_2 into nascent X is given by,



where C_o is the initial concentration of X_2 , a the degree of dissociation and k is the unimolecular dissociation rate constant. The net rate of formation of X is,

$$\dot{C}_X = kC_{X_2} - (k/K_c)C_X^2, \quad (2)$$

where K_c is the concentration equilibrium constant of reaction (1) and C_{X_2} and C_X are the concentrations of X_2 and X, respectively. At equilibrium, $\dot{C}_X = 0$, and it follows from eq. (2) that,

$$K_c = \left(\frac{C_X^2}{C_{X_2}} \right)_e = \frac{4a_e^2}{1-a_e} C_o, \quad (3)$$

where the subscript e refers to the equilibrium values.

Let the total volume of the system be V ; at $t = 0$, $V = V_o$. Dissociation occurs at constant pressure (say, 1 atm) if at time t ,

$$V = V_o(1 + a), \quad a = a(t). \quad (4)$$

The conservation relation at time t is,

$$C_o V_o = \left(C_{X_2} + \frac{C_X}{2} \right) V, \quad (5)$$

and from the definition of a ,

$$C_{X_2} V = C_o V_o (1 - a) . \quad (6)$$

It follows from eqs. (4), (5) and (6) that,

$$C_{X_2} = C_o \frac{1 - a}{1 + a} , \quad (7)$$

and

$$C_X = 2C_o \frac{a}{1 + a} , \quad (8)$$

which lead to the familiar equilibrium expressions for the mole fractions.

From eqs. (2), (7) and (8),

$$\frac{k}{2} dt = \frac{da}{1 - a} \frac{2}{a^2} \quad (9)$$

where,

$$a^2 = 1 + \frac{4C_o}{K_c} . \quad (10)$$

Equations (3) and (10) yield,

$$a = (1 - a_e + a_e^2)^{1/2} / a_e . \quad (11)$$

Integrating eq. (9) and using the boundary condition that $a = 0$ at $t = 0$, one obtains,

$$kt = \frac{1}{a} \ln \frac{1 + a a_e}{1 - a a_e} . \quad (12)$$

Table 1 contains a summary of the results on the dissociation of the halogens at 1000 and 2000°K. From eq. (12), the value of $t_{1/2}$, the time required for a to reach the value of $(1/2)a_e$, is calculated.

TABLE 1
Dissociation of X_2 at 1000 and 2000°K

X_2	D, (a)	$100a_e$ (a)		ν , (b) s^{-1}	k , s^{-1} (c)		$t_{1/2}$, s	
	kcal	1000°K	2000°K		1000°K	2000°K	1000°K	2000°K
F_2	38.0	4.3	99.0	2.68×10^{13}	1.33×10^5	1.89×10^9	3.5×10^{-7}	5.7×10^{-10}
Cl_2	57.2	0.035	52.0	1.69×10^{13}	5.35	9.51×10^6	7.1×10^{-5}	5.9×10^{-8}
Br_2	45.4	0.23	72.4	0.97×10^{13}	1.16×10^3	1.06×10^8	2.2×10^{-6}	7.4×10^{-9}
I_2	35.5	2.8	89.5	0.64×10^{13}	1.12×10^5	8.45×10^8	2.7×10^{-7}	1.2×10^{-9}

- (a) See Table 104 on page 773 of, Treatise on Inorganic Chemistry, by H. Remy, Vol. I (Elsevier, 1956).
 (b) See Table 39 in the Appendix of, Spectra of Diatomic Molecules, by G. Herzberg (Van Nostrand, 1953).
 (c) $k = \nu \exp(-D/RT)$, where ν is the C-X vibrational frequency.

REFERENCES

1. C. J. Duthler, "Extrinsic Absorption in 10.6 μm Laser Window Materials Due to Molecular-Ion Impurities, *J. Appl. Phys.* 45, 2668 (1974).
2. Chemistry of Halide Window Growth, Contract F33615-74-C-5115, Interim Technical Report 1.
3. V. I. Vedeneyev, L. V. Gurvich, V. N. Kondrat'yev, V. A. Medvedev, and Ye L. Frankevich, Bond Energies, Ionization Potentials, and Electron Affinities (St. Martin's Press, 1966).
4. A. H. Schon and M. Szwarc, "The C-Br Bond Dissociation Energy in Halogenated Bromomethanes," *Proc. Roy. Soc.* A209, 110 (1951).
5. L. J. Bellamy, The Infrared Spectra of Complex Molecules (Wiley, 1956).
6. E. M. Levin, C. R. Robbins, and H. F. McMurdie, Phase Diagrams for Ceramists, 1969 Supplement, p. 396, Fig. 3505 (The American Ceramic Society, Inc. 1969).
7. C. E. Wicks and F. E. Block, Thermodynamic Properties of 65 Elements - Their Oxides, Halides, Carbides, and Nitrides, Bulletin 605, U. S. Bureau of Mines, U. S. Government Printing Office (Washington, 1963).
8. D. R. Stull and H. Prophet in JANAF Thermochemical Tables: Second Edition, NSRDS-NBS 37, U. S. Government Printing Office, Issued June 1973.
9. "Fluoride Window Materials for Use as Laser Windows in the 2 to 6 μm Spectral Region," Contract F33615-73-C-5075. See Fig. 5-2.
10. M. Rolin and M. Clausier, "System Calcium Fluoride-Barium Fluoride-Magnesium Fluoride, II," *Rev. Int. Hautes Temp Refract.* 4, 43 (1967). The eutectic is at 44 wt. % MgF_2 and 980°C.
11. V. T. Berezhnaya and G. A. Bukhalova, "Barium, Calcium and Magnesium Fluorides Ternary Systems," *Russ. J. Inorg. Chem.* 6, 1091 (1961). The eutectic is at 58% MgF_2 and 948°C.
12. P. F. Weller, J. D. Axe, and G. D. Petit, "Chemical and Optical Studies of Samarium Doped CaF_2 Type Single Crystals," *J. Electrochem. Soc.* 112, 74 (1965).

13. R. H. Nafziger, "High-Temperature Phase Relations in the System BaF_2 - SrF_2 ," *J. Am. Ceram. Soc.* 54, 467 (1971).
14. A. Kahan, "Alkaline Earth Fluoride Windows and Domes," TMLW-21, Solid State Sciences Laboratory, AFCRL, L. G. Hanscom Field (Bedford, Mass.)
15. R. T. Newberg, D. W. Readey, H. A. Newborn, and P. A. Miles, "Fusion Casting of Alkaline-Earth Fluoride Laser Optics," Proceedings of the Fourth Annual Conference on Infrared Laser Window Materials (November 18-20, 1974, Tucson, Arizona), Compiled by C. R. Andrews and C. L. Strecker, sponsored by Advanced Research Projects Agency, Issued Jan. 1975.
16. E. G. Chernevskaya and Z. N. Korneva, "The Production of Fluorite Crystals in an Atmosphere Containing Fluorine," *Sov. J. Opt. Tech.* 39, 213 (1972).
17. P. L. McGeer and H. C. Dues, "Effect of Pressure on the Melting Point of Teflon Tetrafluoroethylene Resin," *J. Chem. Phys.* 20, 1813 (1952). From the dependence of melting temperature on pressure, PTFE melts at $324^{\circ}C$ at atmospheric pressure.
18. Hanford and Joyce, "Polytetrafluoroethylene," *J. Am. Chem. Soc.* 68, 2082 (1946). Using optical methods to determine the disappearance of the last crystallites, they obtain $327^{\circ}C$ as the melting point of PTFE.
19. J. C. Siegle and L. T. Muus, "Pyrolysis of Polytetrafluoroethylene," 130th American Chemical Society Meeting, Sept. 1956.
20. E. E. Lewis and M. A. Naylor, "Pyrolysis of Polytetrafluoroethylene," *J. Am. Chem. Soc.* 69, 1968 (1947).
21. M. Hass, J. W. Davisson, H. B. Rosenstock, J. A. Slinkman, and J. Babiskin, Optical Properties of Highly Transparent Solids, S. S. Mitra and B. Bendow, Eds. Optical Physics and Engineering Series edited by W. L. Wolfe (Plenum Press, 1975).